Available online at www.sciencedirect.com
SCIENCE DIRECT®
Geochimica et Cosmochimica Acta 70 (2006) 3401–3420
Geochimica
www.elsevier.com/locate/gca

Subduction and melting processes inferred from U-Series, Sr–Nd–Pb isotope, and trace element data, Bicol and Bataan arcs, Philippines

S. Andrew DuFrane [a,*], Yemane Asmerom [a], Samuel B. Mukasa [b], Julie D. Morris [c], Brian M. Dreyer [c]

[a] *University of New Mexico, Department of Earth & Planetary Sciences, Albuquerque, NM, USA*
[b] *University of Michigan, Department of Geological Sciences, Ann Arbor, MI, USA*
[c] *Washington University, Department of Earth & Planetary Science, St. Louis, MO, USA*

Received 13 June 2005; accepted in revised form 21 April 2006

Abstract

We present U-series, Sr–Nd–Pb isotope, and trace element data from the two principal volcanic chains on Luzon Island, developed over oppositely dipping subduction zones, to explore melting and mass transfer processes beneath arcs. The Bataan (western) and Bicol (eastern) arcs are currently subducting terrigenous and pelagic sediments, respectively, which have different trace element and isotopic compositions. The range of (^{230}Th/^{238}U) disequilibria for both arcs is 0.85–1.15; only lavas from Mt. Mayon (Bicol arc) have ^{230}Th activity excesses. Bataan lavas have higher ^{87}Sr/^{86}Sr and lower ^{143}Nd/^{144}Nd than Bicol lavas (^{87}Sr/^{86}Sr = 0.7042–0.7046, ^{143}Nd/^{144}Nd = 0.51281–0.51290 vs. ^{87}Sr/^{86}Sr = 0.70371–0.70391, ^{143}Nd/^{144}Nd = 0.51295–0.51301) and both arcs show steep linear arrays towards sediment values on ^{207}Pb/^{204}Pb vs. ^{206}Pb/^{204}Pb diagrams. Analysis of incompatible element and isotopic data allows identification of a sediment component that, at least in part, was transferred as a partial melt to the mantle wedge peridotite. Between 1% and 5% sediment melt addition can explain the isotopic and trace element variability in the rocks from both arcs despite the differences in sediment supply. We therefore propose that sediment transfer to the mantle wedge is likely mechanically or thermally limited. It follows that most sediments are either accreted, reside in the sub-arc lithosphere, or are recycled into the convecting mantle. However, whole-sale sediment recycling into the upper mantle is unlikely in light of the global mid-ocean ridge basalt data. Fluid involvement is more difficult to characterize, but overall the Bicol arc appears to have more fluid influence than the Bataan arc. Rock suites from each arc can be related by a dynamic melting process that allows for ^{230}Th ingrowth, either by dynamic or continuous flux melting, provided the initial (^{230}Th/^{232}Th) of the source is ~0.6–0.7. The implication of either model is that inclined arrays on the U–Th equiline diagram may not have chronologic significance. Modeling also suggests that U-series disequilibria are influenced by the tectonic convergence rate, which dictates mantle matrix flow. Thus with slower matrix flow there is a greater degree of ^{230}Th ingrowth. While other factors such as prior mantle depletion and addition of a subducted component may explain some aspects of U-series data, an overall global correlation between tectonic convergence rate and the extent of U–Th disequilibria may originate from melting processes.
© 2006 Elsevier Inc. All rights reserved.

1. Introduction

Over the past three decades much progress has been made in identifying the source components that contribute to arc lavas. These include mantle peridotite and subducted oceanic lithosphere with overlying sediments (Tera et al., 1986; Morris and Tera, 1989). While there is general consensus about which components are involved, less is understood about the processes that govern their elemental and isotopic contributions to the magmas which are produced.

In contrast to melting beneath mid-ocean ridges (MOR) and ocean islands (OI) melting processes beneath island arcs are poorly constrained. The aqueous flux of elements from the subducting slab, thought to trigger major mantle melting, is well documented by large ion lithophile element (LILE) relative to high field strength element (HFSE) ratios in arc lavas (e.g., Tatsumi et al., 1986;

* Corresponding author.
E-mail address: radium@unm.edu (S.A. DuFrane).

0016-7037/$ - see front matter © 2006 Elsevier Inc. All rights reserved.
doi:10.1016/j.gca.2006.04.020

Tatsumi, 1989; Elliott et al., 1997; Class et al., 2000). However, it is not clear whether the degree of melting is entirely controlled by the fluid flux or whether there is an additional decompression melting component. Both major/trace element studies (Plank and Langmuir, 1988; Pearce and Parkinson, 1993) and numeric models (Davies and Stevenson, 1992; Kincaid and Sacks, 1997; Hall and Kincaid, 2001) have inferred that upwelling in the mantle wedge may induce partial melting, and yet disentangling the relative importance of flux-driven vs. decompression melting with geochemical data-sets has proven to be a nontrivial task.

U-series isotopes are potentially useful time-sensitive indicators of recent fluid enrichment and partial melting processes because of their short half lives and the varied geochemical behaviors of the daughter elements in the series. ^{238}U decays to ^{234}U, which then decays to ^{230}Th ($t_{1/2} = 75{,}690$ yrs, Cheng et al., 2000) and ^{226}Ra ($t_{1/2} = 1599$ yrs, Holden, 1990). ^{235}U decays to ^{231}Pa ($t_{1/2} = 32{,}760$ yrs, Robert et al., 1969). The activity (number of atoms times decay constant) ratio of any parent–daughter nuclide pair is unity when secular equilibrium has been established. Deviation from unity can result from recent mineral-melt partitioning, fluid addition of soluble elements, ingrowth, and decay; however, the activity ratio of a parent–daughter nuclide pair returns to unity within ~5 half-lives of the shortest-lived nuclide.

Arc magmas commonly have (^{238}U/^{230}Th) and (^{226}Ra/^{230}Th) activity ratios >1, which is generally attributed to greater solubility of U and Ra compared to Th in subduction zone fluids (Gill and Williams, 1990; Brenan et al., 1994, 1995b; Keppler, 1996). Recent studies have demonstrated the potential of U-series disequilibria for quantifying the timescales of fluid addition beneath arcs with extensively depleted mantle wedges (Bourdon et al., 1999; Turner et al., 1997, 2000, 2001). In these instances aqueous induced element fluxes are amplified. However, in arcs that do not have back-arc spreading centers, including the Philippines, it is not clear if melting processes have a more pronounced effect on U-series systematics. ^{230}Th activity excesses are rare in arcs, but common at OIs and MORs where they are interpreted to be the result of both chemical fractionation and radioactive ingrowth of daughter nuclides during decompression partial melting. Also, since Pa, like Th, is thought to be insoluble in aqueous fluids, ^{231}Pa activity excesses found in arc rocks (Pickett and Murrell, 1997) provide strong evidence that partial melting effects can overprint the effects of U addition via fluids. Thus, even in arcs, U-series disequilibria may be useful for investigating the nature of melting processes (Bourdon et al., 1999, 2003; George et al., 2003).

Another issue regarding arc magmatism is the extent to which contribution from a generic "subducted component" can be resolved into discrete additions from oceanic crust and sediments, and whether the nature of element transfer from slab to wedge can be constrained (e.g., as aqueous fluids, silicic partial melts, or in bulk). Understanding such complexities is crucial for attempts to constrain element mass balance between the crust and mantle. Fluid addition is thought to be responsible for the ubiquitous LILE enrichment of arc lavas; however, sediments often have preexisting LILE enrichments and negative Nb anomalies. Moreover, even the presence of an OIB-type component in the mantle wedge has been suggested (Morris and Hart, 1983; Reagan and Gill, 1989; Stolz et al., 1990). In case additions of discrete components can be resolved, information about the relative timing of addition of each component to the mantle wedge can reveal clues about subduction processes. Several authors have argued for a single subduction component that triggers extensive mantle melting (e.g., Tatsumi et al., 1986; Tatsumi, 1989). Yet experimental studies suggest that dehydration reactions occur over a range of pressures and therefore, multiple subduction components could be transferred discretely or continuously prior to major mantle melting. Thus understanding the absolute and relative timing of mass transfer processes beneath arcs has remained a major challenge to date (Hawkesworth and Ellam, 1989; Hawkesworth et al., 1997; Turner et al., 1997; Turner and Foden, 2001).

To address some of the issues mentioned above, we measured incompatible element concentrations and U-series, Sr, Nd, and Pb isotope ratios of lavas from the Bicol and Bataan arcs, Philippines (Fig. 1). The two arcs have developed over oppositely dipping subduction zones and have contrasting sediment types available for subduction: the Philippine Sea Plate (Bicol arc) has thin pelagic sediments and the South China Sea Plate (Bataan arc) has thick ter-

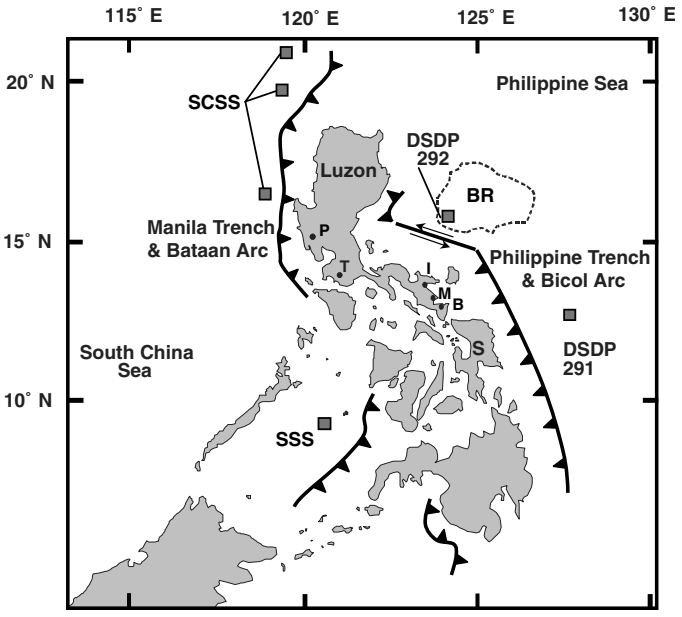

Fig. 1. Tectonic sketch map of the Philippine Archipelago showing the volcanic centers sampled, location of convergent margins, and approximate location of deep sea drill holes discussed in the text. Abbreviations are as follows: I = Iriga, M = Mayon, B = Bulusan, P = Pinatubo, T = Taal, S = Samar, BR = Benham Rise, SCSS = South China Sea sediments, SSS = Sulu Sea sediments, DSDP 219 = Deep Sea Drilling Project drill-hole 291, DSDP 292 = Deep Sea Drilling Project drill-hole 292.

rigenous sediments (McDermott et al., 1993; Solidum, 2002; Castillo and Newhall, 2004). A comprehensive data-set and the unique tectonic setting allow us to resolve fluid and sediment components in each arc. With U-series data we place constraints on the potential effects of decompression partial melting and relate slab dynamics to the rate of melting.

2. Geologic setting and sample descriptions

The Philippine island of Luzon is bounded by the Manila Trench to the west and the Philippine Trench to the east (Fig. 1), both of which are associated with subduction of oceanic lithosphere. The Manila Trench has probably been active since late Oligocene to mid-Miocene era with a long term average subduction rate of 2.5–3 cm yr^{-1} (Hayes and Lewis, 1984). Fault mechanism solutions indicate northeast-directed under-thrusting at 38° dip, and the Wadati-Benioff zone increases to near vertical beneath Taal (Miklius et al., 1991). Lead isotope studies have shown that basalts from the Bataan arc and South China Sea Plate have high $^{207}Pb/^{204}Pb$ and $^{208}Pb/^{204}Pb$ for a given $^{206}Pb/^{204}Pb$ (Mukasa et al., 1987, 1994; Tu et al., 1992; Castillo, 1996), consistent with an Indian Ocean-type affinity (Hart, 1984).

In contrast, the Bicol arc is associated with westward subduction of the Philippine Sea Plate with thin to modest amounts of pelagic sediments and has probably been active for a much shorter period on the basis of a short Wadati-Benioff zone length (120–230 km) and lack of Quaternary volcanism on the island of Samar (Cardwell et al., 1980; Besana et al., 1997). Little geophysical work has been published to constrain the geometry of the down-going slab, although seismic data indicate a relatively shallow subduction system dipping 24° at the northern end of the Philippine Trench (Cardwell et al., 1980). The estimated convergence rate for the Philippine Sea Plate is approximately 4.8–6.4 cm yr^{-1} based on NUVEL1 and NUVEL1a plate motion calculators (Hamburger et al., 1983; Argus and Gordon, 1991; DeMets et al., 1994).

Samples for this study are from five different volcanic centers: Taal and Pinatubo in the Bataan arc, and Mayon, Iriga, and Bulusan in the Bicol arc (Fig. 1). The samples range in composition from basalt to dacite. Three volcanoes—Pinatubo, Taal, and Mayon—have well constrained historic eruption ages: Pinatubo erupted in 1991 and 4000 ybp (Newhall et al., 1996); Taal has been active since the early 1600 s; and Mayon has erupted every ~15–20 yrs since the late 19th century to the present and has probably been active since the Pleistocene (Ramos-Villarta et al., 1985). Eruption ages from Iriga are not as well constrained, but are certainly Holocene in age (Aguila et al., 1986; Delfin et al., 1993). Some historical records suggest Iriga was active during the early to mid-1600s but this is unconfirmed (Aguila et al., 1986). The present Bulusan Volcanic Complex has been active since the Pleistocene, and volcanic activity has been divided into pre-caldera (1.1 Ma–40 ka), caldera (40–35 ka), and post-caldera stages (35 ka–present) (Delfin et al., 1993). Our samples are from Bulusan's most recent volcanic activity, which commenced at ~6 ka.

3. Analytical methods

U–Th purification and mass spectrometry were accomplished at the Radiogenic Isotope Laboratory, University of New Mexico using methods described in Asmerom and Edwards (1995) and Asmerom (1999). Briefly, 0.1–0.2 g of whole rock powder were dissolved in PFA bombs in an $HF–HNO_3$ solution at 110 °C for 24–48 h. The solution was then transferred to a 30 ml PFA beaker containing a known quantity of mixed ^{229}Th, ^{233}U, ^{236}U tracer and fluxed with perchloric and boric acids to ensure sample spike equilibration and breakdown of fluoride compounds. Before column separation, U and Th were co-precipitated with iron hydroxides by adjusting the pH of the dissolved solution with aqueous NH_4OH. Samples were centrifuged, the NH_4OH solution decanted, and the remaining $Fe(OH)_3$ cleaned several times by adding ultra pure water, agitating, then re-centrifuging and decanting the water. Finally the cleaned $Fe(OH)_3$ was dissolved in 7 N HNO_3 for loading onto anion exchange columns filled with Biorad AG X1 resin.

After column separation and purification, U and Th were dissolved in 6N HCl and loaded onto zone-refined Re single filaments using graphite and sintered Re powder as an emitter substrate. U and Th isotopic ratios were measured on a Micromass sector 54 thermal ionization mass spectrometer equipped with a Daly ion counter and a WARP energy filter. With a ^{238}U ion beam, the abundance sensitivity at masses 237 and 236 is 20 and ~2 ppb, respectively, which makes the ^{232}Th tail correction on ^{230}Th unnecessary. Estimated Th and U blanks were 5 and 10 pg, respectively. Samples were background and blank-corrected, although the corrections are negligible.

Sr, Nd, and Pb isotope ratios were measured by thermal ionization mass spectrometry at the University of Michigan, Geochronology and Isotope Geochemistry Laboratory. The samples were processed using standard dissolution and chemical separation procedures described in Mukasa et al. (1987) and Miklius et al. (1991). After column chemistry, each sample was dried to a solid, treated with a drop of 14 N HNO_3, re-dried, and then loaded on appropriate filaments (single rhenium for Pb and Sr, and triple rhenium for Nd). Lead was loaded with a silica gel-phosphoric acid solution, Sr with tantalum solution prepared by dissolving $TaCl_4$ in ultra-pure water, and Nd with 10% nitric acid. Lead isotopic compositions were corrected for fractionation using a factor of 0.12 ± 0.02 percent per AMU, based on the reproducibility of runs for the NIST SRM-981 Pb standard ($n = 10$) during analysis of the samples for this study. Nd and Sr ratios were normalized to $^{146}Nd/^{144}Nd = 0.721900$ and $^{86}Sr/^{88}Sr = 0.119400$, respectively. Measurements for NIST SRM-987 and the La Jolla Nd standard give $^{87}Sr/^{86}Sr = 0.710245 \pm 10$ ($n = 12$, $2\sigma_m$)

and $^{143}Nd/^{144}Nd = 0.511842 \pm 10$ ($n = 12$, $2\sigma_m$), respectively. Total blanks measured once with each nine-sample batch of dissolutions are consistently 0.04 ng for Pb, 0.02 ng for Nd, and 0.1 ng for Sr, all largely controlled by the purity of our reagents, and are inconsequential to the isotopic ratios in this study because of the high concentrations of Pb, Sr and Nd in the samples.

Trace element concentrations were measured with a Fisons Instruments PQ-2 ICP-MS at the University of New Mexico. Approximately 0.100 g of whole-rock sample was digested with HF–HNO_3 in sealed PFA bombs for 24–48 h. The dissolved sample was transferred to a 30 ml PFA beaker, dried to a solid, and re-diluted with 6 ml 3.5 N HNO_3. Samples were fluxed for several hours until completely dissolved, then diluted 1500–3000 times their original weight with In and Re added to achieve a final concentration of 100 ppb In and Re as internal standards. All samples were sonicated for ~30 min prior to analysis. Instrument sensitivity was approximately 5000–15000 cps ppb^{-1} for ^{115}In and ^{187}Re. Whole rock standards USGS RGM-1 (rhyolite) and USGS AGV-1 (andesite) were analyzed during each session. If measured standard values for an element consistently deviated from the accepted value, unknowns were normalized to that percent deviation for the standard in that particular run. Data collected for whole rock standards are reported in Table 2, including 1σ standard deviations, which for most elements are <5%. Effects of correcting the unknown value by normalizing to the standard were negligible for most elements. However, for some elements, particularly the heavy rare earth elements, the correction was significant. No oxide correction was performed for the rare earth elements.

4. Results

4.1. U-series isotopes

U–Th isotope measurements of lavas from this study are shown in Table 1. With the exception of those from Mayon, the lavas all have $(^{230}Th/^{238}U) < 1$, consistent with observations for arcs the world over (Williams and Gill, 1989; Gill and Williams, 1990). Mayon lavas have slight to moderate ^{230}Th activity excesses of 1.06–1.15. Bataan arc lavas generally have lower $(^{230}Th/^{232}Th)$ values than those from the Bicol arc (0.85–1.03 and 0.76–0.88, respectively), although there is some overlap. Lavas from both arcs have relatively low $(^{230}Th/^{232}Th)$ activities compared to average MORB (~1.25).

4.2. Major and trace elements—Sr–Nd–Pb isotopes

Major and trace element data are presented in Table 2. The lavas from this study show a compositional range from basalt to rhyolite and plot within the field for calc-alkaline suites (Fig. 2). The incompatible element distribution diagram, Fig. 3, shows an enrichment spike for Sr and a depletion trough for Nb, characteristic of arc lavas. Also plotted in Fig. 3 are sediment data from the South China Sea and Philippine Sea Plates (McDermott et al., 1993; Solidum, 2002; Castillo and Newhall, 2004), clearly exhibiting Sr enrichment and Nb depletion although not to the same extreme as the lavas.

Sr, Nd, and Pb isotope ratios (shown in Table 2) are broadly similar for the two arcs when compared to the overall mantle array, but the subtle differences between arcs are consistent and significant. Samples from the Bicol arc invariably have the most radiogenic Nd and least radiogenic Sr when compared to samples from the Bataan arc (Fig. 4). Moreover, the Bicol arc volcanoes Mayon and Iriga have very uniform Sr and Nd isotope compositions compared to the Bataan arc volcanoes. Within the Bicol arc itself, Mayon has the highest $^{143}Nd/^{144}Nd$ values compared with Iriga and Bulusan though there is some overlap (Fig. 4). For the Bataan suite, lavas from Taal have lower Nd and higher Sr isotope ratios compared to those from Mt. Pinatubo.

Pb isotope ratios are plotted in Fig. 5, and they show that Bicol and Bataan suites form steep linear arrays between the Northern Hemisphere Regression Line (NHRL) (Hart, 1984) representing the mantle and the fields for Philippine Sea and South China Sea sediment. The spread in $^{207}Pb/^{204}Pb$ values is slightly larger in the Bataan suite, and although three samples approach the NHRL, overall this is a more radiogenic suite than the rocks from the Bicol arc. In fact, the Bicol arc samples actually straddle the NHRL where two samples from Iriga plot slightly below the NHRL on the $^{207}Pb/^{204}Pb$ vs. $^{206}Pb/^{204}Pb$ diagram (Fig. 5b). As demonstrated previously by Mukasa et al. (1987, 1994) and Castillo (1996), Philippine lavas universally display elevated $^{208}Pb/^{204}Pb$ values compared to the NHRL (Fig. 5a), a feature attributed to a time-integrated record of elevated Th/U, similar to the DUPAL isotopic anomaly of the Indian Ocean region (Hart, 1984).

Bicol lavas with the highest $^{143}Nd/^{144}Nd$ and lowest $^{87}Sr/^{86}Sr$ isotope compositions have the highest, albeit moderate, Ba/Th ratio (Fig. 6). In contrast, Bataan lavas have lower $^{143}Nd/^{144}Nd$ and higher $^{87}Sr/^{86}Sr$ for a given Ba/Th ratio. In particular, it is interesting that the Mayon suite has among the highest Ba/Th ratios of all samples measured (only Iriga has higher Ba/Th), and yet U-series data show ^{230}Th activity excesses.

5. Discussion

5.1. Sediment and fluid addition beneath the Bicol and Bataan arcs

5.1.1. Sediment addition

Rock suites from Taal and Pinatubo (Bataan arc) have low $^{143}Nd/^{144}Nd$ and high $^{87}Sr/^{86}Sr$ isotope ratios compared to those from the Bicol arc and show steep linear arrays in $^{207}Pb/^{204}Pb$, $^{208}Pb/^{204}Pb$ vs. $^{206}Pb/^{204}Pb$ diagrams towards values for South China Sea sediment. This is consistent with several studies of Taal and neighboring

Table 1
Th and U element and isotope data for Bicol and Bataan arcs

Sample #	U (ppm)	Th (ppm)	$^{232}Th/^{238}U$	$(^{230}Th/^{232}Th)$	$(^{238}U/^{232}Th)$	$(^{230}Th/^{238}U)$	$(^{234}U/^{238}U)$
Taal							
T1	0.944 ± 5	3.364 ± 9	3.68 ± 2	0.789 ± 8	0.852 ± 5	0.927 ± 10	1.005 ± 7
T2	1.526 ± 6	5.459 ± 26	3.70 ± 2	0.784 ± 12	0.848 ± 5	0.925 ± 14	0.997 ± 4
T3	3.485 ± 15	11.91 ± 6	3.53 ± 2	0.822 ± 9	0.887 ± 6	0.927 ± 10	0.999 ± 2
T4	0.974 ± 5	3.428 ± 12	3.64 ± 2	0.771 ± 9	0.862 ± 6	0.895 ± 11	0.995 ± 7
T5	1.230 ± 4	4.399 ± 14	3.70 ± 2	0.783 ± 6	0.849 ± 4	0.923 ± 7	1.000 ± 3
T23	1.095 ± 4	3.396 ± 22	3.21 ± 2	0.786 ± 8	0.978 ± 7	0.804 ± 7	0.999 ± 3
MB-5 Phil	1.031 ± 50	3.712 ± 21	3.72 ± 3	0.773 ± 7	0.843 ± 6	0.917 ± 8	0.997 ± 5
BAL-1 Phil	3.741 ± 14	12.95 ± 7	3.58 ± 2	0.824 ± 6	0.876 ± 6	0.941 ± 6	0.999 ± 3
BM-8 Phil	3.586 ± 20	12.429 ± 12	3.58 ± 4	0.832 ± 12	0.876 ± 10	0.951 ± 12	1.004 ± 6
CAL-1 Phil	1.030 ± 5	3.793 ± 43	3.80 ± 5	0.762 ± 19	0.824 ± 10	0.924 ± 21	0.999 ± 3
B-4 Phil	0.963 ± 4	3.463 ± 19	3.72 ± 3	0.797 ± 7	0.844 ± 6	0.945 ± 8	1.000 ± 5
CY-3 Phil	1.197 ± 5	4.331 ± 24	3.74 ± 3	0.785 ± 10	0.839 ± 6	0.936 ± 11	0.999 ± 8
Pinatubo							
P16	1.639 ± 5	5.184 ± 19	3.27 ± 2	0.955 ± 8	0.959 ± 5	0.996 ± 8	1.004 ± 7
P17	0.519 ± 2	1.681 ± 5	3.35 ± 2	0.882 ± 9	0.937 ± 4	0.942 ± 9	1.005 ± 4
P18	1.240 ± 13	4.179 ± 17	3.48 ± 4	0.848 ± 13	0.901 ± 10	0.942 ± 17	0.994 ± 12
P19	1.166 ± 4	4.188 ± 16	3.71 ± 2	0.850 ± 10	0.845 ± 5	1.006 ± 12	1.003 ± 4
P20	1.002 ± 4	3.384 ± 13	3.49 ± 2	0.856 ± 11	0.898 ± 5	0.954 ± 13	1.004 ± 4
P20b	1.352 ± 5	4.589 ± 17	3.51 ± 2	0.835 ± 9	0.894 ± 5	0.935 ± 11	1.002 ± 4
P21	1.008 ± 4	3.407 ± 14	3.49 ± 2	0.852 ± 10	0.898 ± 5	0.949 ± 11	0.999 ± 5
P22	1.222 ± 5	3.949 ± 13	3.34 ± 2	0.863 ± 13	0.939 ± 5	0.919 ± 14	0.997 ± 4
Mayon							
M-28	0.612 ± 3	2.241 ± 21	3.78 ± 4	0.951 ± 17	0.829 ± 9	1.148 ± 18	1.005 ± 5
M-38	0.625 ± 2	2.512 ± 8	4.15 ± 2	0.846 ± 9	0.755 ± 4	1.120 ± 12	1.003 ± 3
MY-47 6700	0.568 ± 3	2.231 ± 13	4.06 ± 3	0.863 ± 7	0.773 ± 6	1.117 ± 8	1.002 ± 4
MY-68	0.669 ± 3	2.490 ± 14	3.85 ± 3	0.887 ± 15	0.815 ± 6	1.088 ± 18	1.000 ± 6
MY-78	0.584 ± 3	2.258 ± 13	3.99 ± 3	0.867 ± 7	0.785 ± 6	1.104 ± 9	1.001 ± 5
MY-84	0.623 ± 3	2.356 ± 15	3.90 ± 3	0.876 ± 18	0.804 ± 6	1.091 ± 22	1.000 ± 4
M8-93	0.619 ± 2	2.344 ± 9	3.91 ± 2	0.850 ± 11	0.802 ± 4	1.060 ± 14	0.999 ± 4
M7-00	0.599 ± 2	2.219 ± 8	3.83 ± 2	0.873 ± 13	0.819 ± 4	1.066 ± 16	1.005 ± 4
M6-01	0.596 ± 2	2.034 ± 7	3.53 ± 2	0.939 ± 7	0.889 ± 4	1.056 ± 10	1.006 ± 4
Bulusan							
B9	1.055 ± 4	3.114 ± 8	3.05 ± 2	0.985 ± 7	1.028 ± 5	0.958 ± 7	1.004 ± 5
B10	1.136 ± 4	3.452 ± 10	3.14 ± 2	0.959 ± 8	0.999 ± 5	0.961 ± 9	1.002 ± 5
B11	1.292 ± 5	4.034 ± 15	3.23 ± 2	0.956 ± 11	0.971 ± 5	0.984 ± 11	0.998 ± 4
Iriga							
I12	0.941 ± 3	2.880 ± 9	3.16 ± 2	0.918 ± 8	0.992 ± 5	0.926 ± 9	1.001 ± 4
I13	0.706 ± 3	1.784 ± 12	2.61 ± 2	0.994 ± 11	1.201 ± 10	0.828 ± 8	1.011 ± 7
I14	0.699 ± 3	1.867 ± 5	2.76 ± 2	0.943 ± 8	1.136 ± 6	0.830 ± 8	0.983 ± 7
I15	0.712 ± 2	1.739 ± 5	2.52 ± 1	1.032 ± 10	1.243 ± 5	0.830 ± 9	1.009 ± 4

All uncertainties are 2σ measurement errors. Our U and Th spikes were calibrated using standards prepared from pure U and Th metals. Intra-laboratory calibrations were done by measuring Table Mountain Latite rock standard (Asmerom, 1999) and cross calibrations with the University of Minnesota using spikes, standards, and secular equilibrium samples (Cheng et al., 2000). Our spike U and Th values were checked periodically throughout this study. Repeated measurement of NBL-112 U standard yielded a $\delta^{234}U$ of $-37.69 \pm 0.53‰$ ($n = 64$, error $= 2\sigma$ external) in agreement with previously published values of $-37.1 \pm 1.2‰$ (Edwards et al., 1993) and $-36.9 \pm 2.1‰$ (Cheng et al., 2000). The decay constant used to calculate $^{234}U/^{238}U$ activities is that of Cheng et al. (2000). Measurements of an in house mixed Th/U metal standard over the study period yielded 505.2 ± 2.1 ng/g ($n = 13$) and 193.16 ± 0.31 pg/g ($n = 24$) for Th and U, respectively, where the expected values are 504.02 ng/g and 193.03 pg/g.

volcanic centers that have shown that sediment addition has modified the Bataan sub-arc mantle (Mukasa et al., 1987, 1994; Castillo, 1996; Castillo and Newhall, 2004; Knittel et al., 1997). Also, Bataan lavas have low Ba/Th ratios (50–100) for a given $^{87}Sr/^{86}Sr$ and $^{143}Nd/^{144}Nd$. To first order, low Ba/Th ratios are consistent with sediment addition to the mantle wedge in some fashion as has been convincingly shown for arcs that have high sediment fluxes, such as the southern Lesser Antilles and Sunda arcs (see Fig. 6). Also, Th/La correlates well with Nd isotope ratios whereby lavas with low $^{143}Nd/^{144}Nd$ have high Th/La (Fig. 7a). High Th/La in arc lavas is a characteristic likely inherited from subducted sediments (Plank, 2005), which typically have Th/La > 0.2. There are no La and Th data reported for South China Sea and Sulu Sea sediments, and therefore Global Subducted Sediment (GLOSS) (Plank and Langmuir, 1998) is shown for comparison in Figs. 7 and 8a. Combined with basalts from the Macolod Corridor the data form a broad trend towards Th/La > 0.5, notably higher than GLOSS. Individual volcanic centers trend to

Table 2
Major element oxide, trace element, and Sr–Nd–Pb isotope data for Bicol and Bataan arcs

Sample ID (volcano)	M28 (Mayon)	M38 (Mayon)	M47-6700 (Mayon)	M47-MT (Mayon)	M68 (Mayon)	M78 (Mayon)	M84 (Mayon)	M8-93 (Mayon)	M7-00 (Mayon)
SiO_2[a]	55.13	55.48	55.47	55.91	54.54	55.06	56.53	52.98	53.86
TiO_2	0.72	0.71	0.74	0.73	0.73	0.70	0.75	0.71	0.71
Al_2O_3	20.17	20.96	19.36	19.95	20.27	20.02	19.44	18.29	19.15
Fe_2O_3[b]	8.36	8.06	8.64	8.37	8.45	8.34	8.49	8.28	8.13
MnO	0.17	0.17	0.18	0.18	0.17	0.17	0.18	0.17	0.16
MgO	4.30	4.16	4.58	4.29	4.43	4.35	4.44	4.14	4.14
CaO	8.58	8.43	8.59	8.45	8.39	8.76	8.38	8.27	8.44
Na_2O	3.63	3.62	3.55	3.69	3.52	3.58	3.62	3.45	3.43
K_2O	1.17	1.17	1.13	1.19	1.17	1.12	1.21	1.14	1.09
P_2O_5	0.28	0.29	0.29	0.30	0.28	0.28	0.30	0.28	0.28
Sr[c]	668	667	669	672	652	699	684	641	690
Ba	354	363	352	369	347	352	371	354	359
La	15.3	15.3	14.9	16.0	15.0	14.4	15.6	15.1	14.9
Ce	34.3	34.3	32.9	34.9	33.5	32.3	34.8	33.6	33.8
Pr	4.3	4.3	4.2	4.4	4.2	4.1	4.4	4.3	4.3
Nd	17.4	17.4	17.2	17.8	17.4	16.7	17.7	17.5	17.5
Sm	3.8	3.9	3.8	4.0	3.9	3.8	4.0	3.9	3.9
Eu	0.96	0.96	0.95	0.99	0.93	0.94	0.97	0.92	0.95
Gd	3.5	3.4	3.4	3.5	3.3	3.3	3.5	3.3	3.3
Tb	0.6	0.6	0.7	0.7	0.6	0.6	0.7	0.6	0.6
Er	2.4	2.4	2.4	2.5	2.4	2.3	2.5	2.5	2.4
Dy	3.7	3.7	3.7	3.8	3.6	3.5	3.8	3.7	3.7
Ho	0.8	0.8	0.8	0.8	0.8	0.8	0.8	0.8	0.8
Yb	1.8	1.9	1.9	1.9	1.9	1.8	2.0	1.9	1.8
Th[d]	2.241	2.512	2.231	—	2.490	2.258	2.356	2.344	2.219
U	0.612	0.625	0.568	—	0.669	0.584	0.624	0.619	0.599
Nb	3.6	3.4	3.2	3.4	3.3	3.2	3.4	1.85	3.3
Ta	0.3	0.3	0.4	0.3	0.2	0.4	0.3	0.3	0.3
$^{143}Nd/^{144}Nd$[e]	0.513012 ± 21	0.513015 ± 20	0.513044 ± 23	0.512996 ± 24	0.512934 ± 20	0.513016 ± 20	0.513002 ± 20	0.512975 ± 19	0.512969 ± 19
$^{87}Sr/^{86}Sr$	0.703715 ± 37	0.703699 ± 37	0.703763 ± 42	0.703732 ± 42	0.703733 ± 40	0.703746 ± 39	0.703749 ± 36	0.703823 ± 11	0.703827 ± 15
$^{206}Pb/^{204}Pb$	18.569	18.544	18.559	18.578	18.556	18.564	18.56418	18.614	18.608
$^{207}Pb/^{204}Pb$	15.542	15.516	15.531	15.551	15.53	15.537	15.52	15.583	15.559
$^{208}Pb/^{204}Pb$	38.401	38.303	38.374	38.433	38.373	38.383	38.323	38.546	38.451

Sample ID (volcano)	M6-01 (Mayon)	B9 (Bulusan)	B10 (Bulusan)	B11 (Bulusan)	I12 (Iriga)	I13 (Iriga)	I14 (Iriga)	I15 (Iriga)	T1 (Taal)
SiO_2	54.11	58.64	59.59	59.66	54.02	50.47	49.82	51.46	50.88
TiO_2	0.71	0.50	0.53	0.51	0.83	0.87	0.89	0.91	0.72
Al_2O_3	18.97	18.15	17.80	18.05	19.63	19.49	19.17	19.63	17.30
Fe_2O_3	8.22	6.30	6.37	6.00	8.37	8.51	8.62	8.96	9.54
MnO	0.16	0.14	0.14	0.13	0.15	0.14	0.14	0.15	0.17
MgO	4.20	3.18	2.96	2.78	4.89	5.47	5.51	5.86	5.81
CaO	8.42	6.93	6.73	6.65	9.14	9.33	9.66	9.80	10.70
Na_2O	3.47	3.40	3.39	3.40	3.61	3.03	2.80	3.08	2.60
K_2O	1.12	1.71	1.75	1.87	1.61	1.31	1.28	1.31	0.90
P_2O_5	0.28	0.18	0.18	0.17	0.31	0.23	0.20	0.21	0.14
Sr	678	429	419	447	969	983	951	954	334
Ba	348	429	430	500	424	357	351	358	211

La	14.2	13.0	13.9	16.0	15.5	10.8	10.3	10.3	9.6
Ce	32.1	26.2	28.4	31.0	34.9	26.0	24.4	24.7	21.4
Pr	4.0	3.0	33	3.4	4.4	3.4	3.2	3.3	2.6
Nd	16.5	11.3	12.6	12.8	17.5	14.3	13.8	13.9	10.6
Sm	3.7	2.5	2.8	2.7	3.9	3.5	3.3	3.4	2.5
Eu	0.93	0.76	0.78	0.82	1.00	0.90	0.88	0.90	0.55
Gd	3.2	2.5	2.7	2.7	3.4	2.9	2.8	2.8	2.6
Tb	0.6	0.4	0.4	0.4	0.6	0.5	0.5	0.5	0.4
Er	2.2	1.3	1.5	1.3	2.1	1.8	1.8	1.9	1.9
Dy	3.4	2.4	2.7	2.5	3.4	3.0	3.0	3.0	3.2
Ho	0.7	0.5	0.6	0.5	0.7	0.6	0.6	0.6	0.7
Yb	1.8	1.4	1.6	1.4	1.7	1.4	1.3	1.4	1.5
Th	2.034	3.114	3.452	4.034	2.880	1.784	1.867	1.739	3.364
U	0.596	1.055	1.136	1.292	0.941	0.706	0.699	0.712	0.944
Nb	3.2	3.6	3.4	4.3	3.8	2.7	2.6	2.6	2.5
Ta	0.3	0.3	0.5	0.4	0.6	0.3	0.3	0.3	0.2
$^{143}Nd/^{144}Nd$	0.512960 ± 20	0.512964 ± 20	0.512973 ± 16	0.512952 ± 18	0.512969 ± 19	0.512966 ± 20	0.512995 ± 13	0.512967 ± 14	0.512842 ± 20
$^{87}Sr/^{86}Sr$	0.703792 ± 13	0.703934 ± 15	0.703913 ± 15	0.703976 ± 11	0.703680 ± 14	0.703753 ± 13	0.703753 ± 13	0.703751 ± 18	0.704572 ± 11
$^{206}Pb/^{204}Pb$	18.574	18.467	18.468	18.476	18.600	18.601	18.560	18.665	18.543
$^{207}Pb/^{204}Pb$	15.562	15.502	15.517	15.520	15.504	15.490	15.518	15.574	15.586
$^{208}Pb/^{204}Pb$	38.526	38.192	38.242	38.345	38.342	38.366	38.450	38.630	38.597

Sample ID (volcano)	T2 (Taal)	T3 (Taal)	T4 (Taal)	T5 (Taal)	T23 (Taal)	BAL1[f] (Taal)	BM8 (Taal)	B4 (Taal)	CAL1 (Taal)
SiO_2	55.57	65.09	50.84	53.87	53.87	64.36	63.81	50.93	51.35
TiO_2	0.89	0.63	0.77	0.82	0.80	0.57	0.6	0.74	0.77
Al_2O_3	17.45	15.87	15.08	17.24	16.02	15.49	15.69	17.15	17.2
Fe_2O_3	9.46	6.06	10.41	9.97	10.84	5.75	6.4	10.18	10.28
MnO	0.18	0.12	0.19	0.18	0.20	0.13	0.14	0.22	0.22
MgO	4.61	1.62	7.07	5.97	7.67	1.97	1.5	5.95	5.65
CaO	9.01	4.34	10.97	10.61	11.78	4.37	4.45	11.03	10.92
Na_2O	3.44	4.18	2.42	2.88	2.59	3.93	4.09	2.69	2.46
K_2O	1.41	2.91	0.90	1.17	0.94	3.27	3.07	0.94	1
P_2O_5	0.22	0.21	0.15	0.18	0.15	0.16	0.24	0.16	0.16
Sr	292	226	301	316	304				
Ba	310	556	214	260	211	573	572	215	220
La	13.9	21.9	9.7	11.6	9.7	21.7	22.13	10.47	11.33
Ce	30.6	45.9	21.8	26.0	22.2	43	44.75	21.68	23.29
Pr	3.7	5.2	2.7	3.1	2.6				
Nd	14.9	19.6	11.0	12.5	10.8	18.2	20	13.3	8.9
Sm	3.5	4.3	2.6	3.1	2.5	4.3	4.6	2.9	3.2
Eu	0.70	0.76	0.5	0.6	0.5				
Gd	3.7	4.7	2.8	3.2	2.6				
Tb	0.7	0.9	0.5	0.5	0.5				
Er	2.8	3.4	2.0	2.2	1.5				
Dy	4.5	5.3	3.4	3.7	3.2				
Ho	1.1	1.4	0.8	0.9	0.7				
Yb	2.1	2.7	1.6	1.7	1.5	2.8	2.9	1.8	1.8
Th	5.459	11.916	3.428	4.399	3.396	12.96	12.43	3.40	3.79
U	1.526	3.485	0.974	1.230	1.095	3.74	3.59	0.96	1.03

(*continued on next page*)

Table 2 (*continued*)

Sample ID (volcano)	T2 (Taal)	T3 (Taal)	T4 (Taal)	T5 (Taal)	T23 (Taal)	BAL1[f] (Taal)	BM8 (Taal)	B4 (Taal)	CAL1 (Taal)
Nb	3.9	6.7	3.2	3.2	3.2				
Ta	0.4	0.5	0.3	0.3	0.2	0.4	0.4	0.2	0.2
$^{143}Nd/^{144}Nd$	0.512844 ± 16	0.512831 ± 19	0.512817 ± 19	0.512837 ± 20	0.512831 ± 190.5128	0.512810 ± 20	0.512830 ± 20	0.512810 ± 20	—
$^{87}Sr/^{86}Sr$	0.704553 ± 13	0.704601 ± 15	0.70449 ± 10	0.704521 ± 11	0.704601 ± 150.7	0.704590 ± 40	0.704580 ± 40	0.704570 ± 20	0.704520 ± 40
$^{206}Pb/^{204}Pb$	18.601	18.580	18.594	18.547	18.580	18.577	18.635	18.581	18.554
$^{207}Pb/^{204}Pb$	15.602	15.577	15.598	15.574	15.570	15.584	15.656	15.614	15.586
$^{208}Pb/^{204}Pb$	38.627	38.581	38.662	38.667	38.558	38.626	38.846	38.729	38.647

Sample ID (volcano)	CY3 (Taal)	MB5 (Taal)	P16 (Pinatubo)	P17 (Pinatubo)	P18 (Pinatubo)	P19 (Pinatubo)	P20 (Pinatubo)	P20b (Pinatubo)	P21 (Pinatubo)
SiO_2	56.38	50.53	63.74	55.11	64.31	63.27	66.38	73.75	65.71
TiO_2	0.85	0.76	0.67	1.17	0.66	0.64	0.60	0.53	0.58
Al_2O_3	10.84	15.28	17.45	17.46	16.90	17.00	18.99	19.43	18.76
Fe_2O_3	10.84	11.06	5.48	8.76	5.71	5.29	4.89	4.39	4.79
MnO	0.28	0.25	0.12	0.15	0.13	0.11	0.11	0.10	0.11
MgO	6.02	7.29	3.16	7.15	4.04	2.98	2.55	2.38	2.47
CaO	11.18	11.38	6.27	10.23	6.08	5.92	5.84	5.45	5.84
Na_2O	2.45	2.4	4.65	3.48	4.51	4.55	4.96	4.93	5.00
K_2O	1.16	0.91	1.69	0.92	1.48	1.44	1.20	1.57	1.20
P_2O_5	0	0.14	0.22	0.21	0.18	0.18	0.18	0.18	0.17
Sr			585	464	511	538	637	556	643
Ba	254	219	443	232	420	422	366	438	369
La	12.14	10.73	17.0	8.6	13.4	14.2	13.4	14.4	13.2
Ce	24.9	22.09	35.8	20.8	29.5	31.0	28.5	30.1	28.5
Pr			4.0	2.7	3.5	3.5	3.3	3.4	3.3
Nd	13.6	10.9	15.2	12.6	13.1	13.3	13.1	13.0	12.5
Sm	3.4	3.0	3.0	3.1	2.7	2.7	2.7	2.4	2.4
Eu			0.7	0.7	0.6	0.6	0.6	0.6	0.6
Gd			3.4	3.2	3.1	3.1	2.8	2.9	2.7
Tb			0.4	0.5	0.4	0.4	0.3	0.3	0.3
Er			1.2	1.5	1.2	1.1	1.0	0.9	0.9
Dy			2.6	3.5	2.5	2.5	2.3	2.2	2.2
Ho			0.5	0.7	0.5	0.4	0.4	0.3	0.4
Yb	2.0	1.9	1.2	1.5	1.1	1.1	1.0	1.0	1.0
Th	4.33	3.71	5.184	1.681	4.179	4.188	3.384	4.589	3.407
U	1.20	1.03	1.639	0.519	1.240	1.166	1.002	1.352	1.008
Nb			4.4	4.1	4.3	4.4	4.0	4.1	3.9
Ta	0.2	0.2	0.3	0.3	0.3	0.3	0.3	0.3	0.3
$^{143}Nd/^{144}Nd$	—	0.512820 ± 20	0.512904 ± 14	0.512923 ± 15	0.51291 ± 18	0.512898 ± 18	0.51291 ± 18	0.512906 ± 20	0.512898 ± 20
$^{87}Sr/^{86}Sr$	0.704580 ± 20	0.704540 ± 20	0.704176 ± 15	0.704207 ± 14	0.704251 ± 10	0.704251 ± 10	0.704213 ± 11	0.704139 ± 14	0.704232 ± 12
$^{206}Pb/^{204}Pb$	18.585	18.639	18.681	18.455	18.394	18.467	18.381	18.404	18.444
$^{207}Pb/^{204}Pb$	15.599	15.668	15.647	15.590	15.624	15.54	15.540	15.545	15.561
$^{208}Pb/^{204}Pb$	38.687	38.867	38.653	38.595	38.400	38.706	38.445	38.70	38.501

Sample ID (volcano)	P22 (Pinatubo)	AGV-1 (standard)	Relative standard deviation (%)	Working value	RGM-1 (standard)	Relative standard deviation (%)	Working value
SiO_2	64.91	—	—	—	—	—	—
TiO_2	0.56	—	—	—	—	—	—
Al_2O_3	17.43	—	—	—	—	—	—
Fe_2O_3	4.57	—	—	—	—	—	—
MnO	0.10	—	—	—	—	—	—
MgO	2.41	—	—	—	—	—	—
CaO	5.27	—	—	—	—	—	—
Na_2O	4.69	—	—	—	—	—	—
K_2O	1.49	—	—	—	—	—	—
P_2O_5	0.17	—	—	—	—	—	—
Sr	570	659.7 (4)	0.94	662	101.72 (4)	0.29	108
Ba	400	1182.4 (4)	0.66	1226	809.91 (4)	0.76	807
La	13.6	38.6 (7)	4.54	38.0	22.3 (7)	3.82	24.00
Ce	29.5	72.0 (7)	4.24	73.0	47.0 (7)	4.50	47.00
Pr	3.3	8.4 (7)	4.75	7.6	5.12 (7)	4.42	4.70
Nd	13.1	30.7 (7)	4.95	33.0	17.9 (7)	5.38	19.00
Sm	2.4	5.53 (7)	5.89	5.9	3.60 (7)	5.20	4.30
Eu	0.6	2.58 (7)	3.34	1.6	1.22 (7)	5.22	0.66
Gd	2.8	6.51 (7)	3.34	5.0	4.00 (7)	3.15	3.70
Tb	0.3	0.57 (7)	5.09	0.7	0.437 (7)	4.50	0.66
Er	1.0	1.73(7)	4.06	1.7	2.02 (7)	3.71	2.60
Dy	2.2	3.17(7)	5.03	3.6	3.14 (7)	4.59	4.08
Ho	0.4	0.487 (7)	8.00	0.67	0.552 (7)	7.16	0.95
Yb	1.0	1.52(7)	4.95	1.72	2.22 (7)	3.58	2.60
Tb	3.949	nd	nd	nd	nd	nd	nd
U	1.222	nd	nd	nd	nd	nd	nd
Nb	4.0	14.9(4)	1.34	15.0	9.61 (4)	1.39	8.90
Ta	0.3	0.98 (4)	4.15	0.90	0.983 (4)	1.55	0.95
$^{143}Nd/^{144}Nd$	0.512900 ± 18	—	—	—	—	—	—
$^{87}Sr/^{86}Sr$	0.704237 ± 11	—	—	—	—	—	—
$^{206}Pb/^{204}Pb$	18.432	—	—	—	—	—	—
$^{207}Pb/^{204}Pb$	15.568	—	—	—	—	—	—
$^{208}Pb/^{204}Pb$	38.518	—	—	—	—	—	—

[a] Major element concentrations were determined by X-ray fluorescence (XRF) on a wavelength dispersive Rigaku RIX 2100 XRF at the Department of Earth and Planetary Sciences, University of New Mexico. Samples were prepared as fused glass disks (1 g sample to 9 g $LiBO_2$ flux). Replicate analyses of whole rock standards BHVO-1 and NBS-278 show estimated precision to be between 0.02% and 1% for all elements. Accuracy for the same standards is estimated to be between 0.1% and 2% for all elements.

[b] Total iron is reported as Fe_2O_3.

[c] Trace elements were determined by ICP-MS using procedures described in the text. Shown are USGS whole rock standards AGV-1 and RGM-1 that were run during the analytical session along with accepted working values (Govindaraju, 1989) and relative standard deviations (n in parentheses); n.d. = not determined.

[d] Th and U were determined by isotope dilution thermal ionization mass spectrometry.

[e] Sr–Nd–Pb isotope ratios were determined using methods described in the text. Errons on Nd and Sr are 2σ. Lead isotopic compositions are corrected for fractionation using a factor of 0.12 ± 0.02 percent per atomic mass unit, based on replicate analyses of NIST SRM-981. Nd and Sr ratios were normalized to $^{146}Nd/^{144}Nd = 0.721900$ and $^{86}Sr/^{88}Sr = 0.119400$, respectively. Measurements for NIST SRM-987 and for the La Jolla Nd Standard give $^{87}Sr/^{86}Sr = 0.710245 \pm 10$, $^{143}Nd/^{144}Nd = 0.511842 \pm 10$, respectively. Total blanks averaged 0.04 ng for Pb, 0.02 ng for Nd, and 0.1 ng for Sr.

[f] Data for samples BAL-1, BM8, B4, CAL1, CY3, and MB5 were previously published in Miklius et al. (1991) and Mukasa et al. (1994).

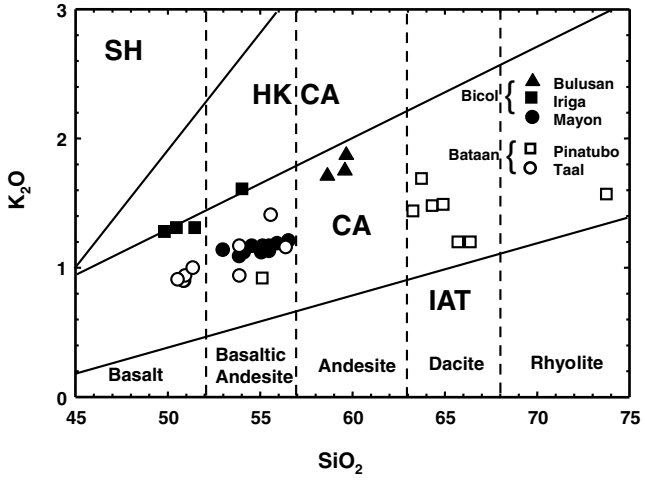

Fig. 2. Plot of K_2O vs. SiO_2 for Bicol and Bataan arc samples from this study. Symbols are explained in the figure legend. Diagonal lines define the following fields: SH, shoshonite; HKCA, high-K calc-alkaline; CA, calc-alkaline; IAT, island arc tholeiite.

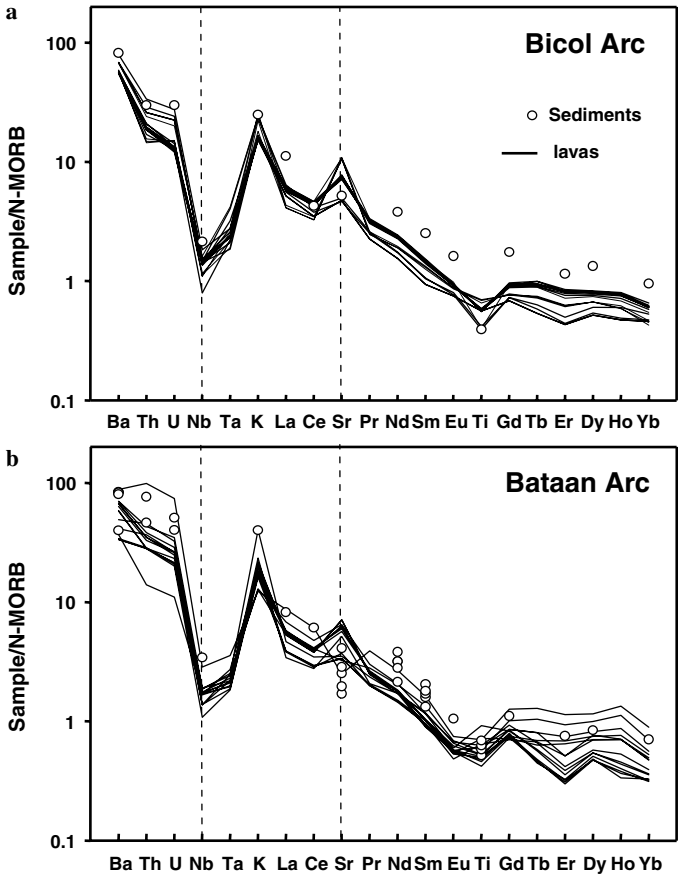

Fig. 3. MORB-normalized incompatible element diagram for (a) Bicol and (b) Bataan arc lavas. Important features include Sr "spikes" and Nb "troughs" shown by the vertical dashed lines. Normalizing values are N-MORB (Sun and McDonough, 1989). Solid lines represent lava compositions from this study and round circles represent sediment data compiled for each arc (McDermott et al., 1993; Solidum, 2002; Castillo and Newhall, 2004).

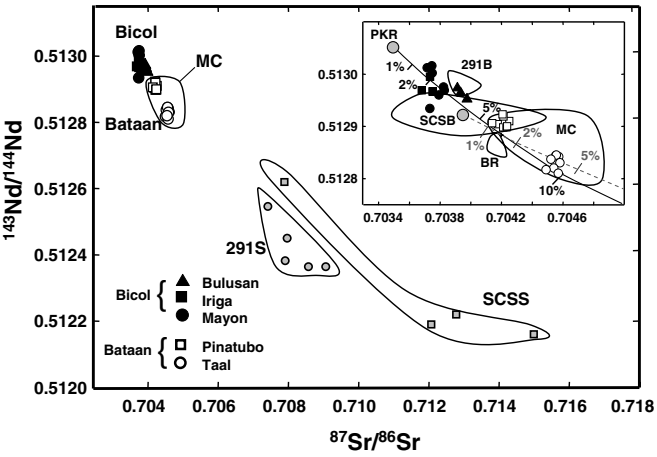

Fig. 4. Sr and Nd isotope ratios for Bicol and Bataan arc lavas. Symbols for the data from this study are explained in the legend. Shown for comparison are data for the South China Sea Sediments (SCSS, grey squares) (McDermott et al., 1993) and Deep Sea Drilling Program drill hole 291 (291S, grey circles) sediments from the West Philippine Sea Basin (Solidum, 2002; Castillo and Newhall, 2004). Inset shows further detail of our data and also includes compositional fields for DSDP hole 291 basalts (291B), Benham Rise (BR), seafloor basalts from the South China Sea (SCSB), and mixing lines between sediments and mantle sources appropriate for each arc (see text for discussion). Solid black line represents mixing between DSDP 291 sediments and a depleted MORB source estimated from the Palau Kyushu Ridge (PKR) (Hickey-Vargas, 1991), while the dashed grey line represents mixing between SCSS and average SCSB. The Bicol arc lavas have higher $^{143}Nd/^{144}Nd$ and lower $^{87}Sr/^{86}Sr$ isotope ratios than those from the Bataan arc which may reflect different mantle sources *and* different sediment compositions. With the differences in source composition taken into account, 1–5% sediment addition arc can explain the data.

higher Th/La at relatively constant $^{143}Nd/^{144}Nd$ (note the Pinatubo data in Fig. 7b). However, most of the Taal samples and all of those from the Macolod Corridor are basaltic-basaltic andesite, and therefore it follows that the *broad* trends to high Th/La in Figs. 7 and 8a are likely a feature of the source rather than from low pressure (crustal) fractionation processes. While low Ba/Th and high Th/La implicates sediment addition, it does not address the mechanism by which the sediment is added to the wedge. For this we use Nd isotopic and Th/Nd, Th/Nb element ratios shown in Figs. 7b and c. In both plots, binary mixing should produce linear trends toward the estimated sediment values. Yet the data arrays broadly trend toward a component with higher Th/Nb and Th/Nd than the sediment estimates. All of the samples from this study are basalt to andesite, except for those from Mt. Pinatubo which are dacites. Even when the Mt. Pinatubo data are excluded the same pattern is maintained, which implies that crustal assimilation processes are an unlikely explanation for the trend. Fractionating Th and Nb is most easily accomplished by partially melting sediments that contain residual phases such as rutile that have high D values for Nb and Nd (Elliott et al., 1997; Class et al., 2000), and therefore if applicable in the Philippine arcs, it is most likely that at least a portion of the sediment component was transferred as a melt phase.

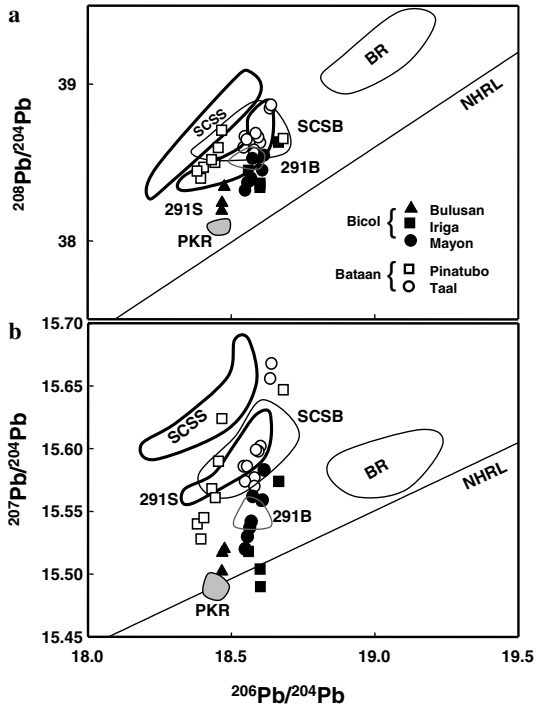

Fig. 5. Pb isotope diagrams for Bicol and Bataan lavas. Symbols for the data from this study are explained in the legend. Shown for comparison are data for South China Sea Sediments (SCSS), South China Sea Basalts (SCSB), Benham Rise (BR), Palau Kyushu Ridge (PKR), DSDP drill-hole 291 sediments (291S) and basalts (291B). Both Bicol and Bataan lavas show steep linear arrays towards values for PSS and SCSS. Also lavas from Iriga plot below the Northern Hemisphere Regression Line (NHRL), close to a mantle domain that is similar to basalts from the Palau Kyushu Ridge (Hickey-Vargas, 1991; McDermott et al., 2005). Data sources are as follows: SCSS (McDermott et al., 1993); SCSB (Tu et al., 1992); 291S (Solidum, 2002; Castillo and Newhall, 2004); 291B, BR and PKR (Hickey-Vargas, 1991, 1998).

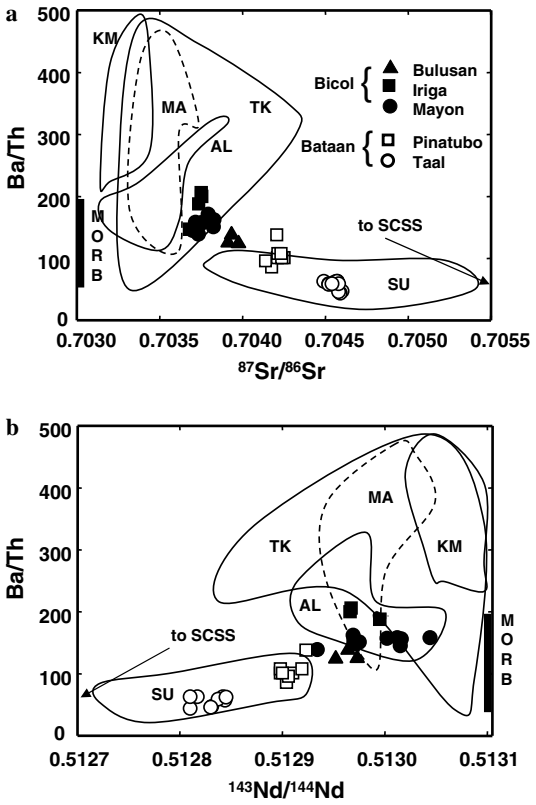

Fig. 6. (a) Ba/Th vs. $^{87}Sr/^{86}Sr$ and (b) Ba/Th vs. $^{143}Nd/^{144}Nd$. Symbols are the same as in Fig. 5. Shown for comparison are compositional fields for Kamchatka (KM), Marianas (MA), Tonga-Kermadec (TK), Aleutians (AL), and Sunda (SU) arcs. Lavas from Bicol and Bataan are well correlated with Sr and Nd isotope ratios and do not exhibit the strong decoupling shown by data from the Marianas, Tonga Kermadec, and Kamchatka. Ba/Th ratios from Tonga extend up to 1200 (not shown). Taal and Pinatubo have the lowest Ba/Th ratios that trend towards values of SCSS and are akin to those from Sunda, Indonesia. Bicol lavas have higher Ba/Th, yet are still in the range of MORB and OIB, which suggests a fluid component (see text for discussion). Data sources are as follows: KM (Turner et al., 1998; Dosseto et al., 2003); MA (Elliott et al., 1997); TK (Turner et al., 1997); AL (George et al., 2003); SU (Turner and Foden, 2001).

Robust compositional estimates of subducted sediment and mantle are necessary to quantify sediment addition and to assess the transfer mechanism of sediments to the mantle wedge peridotite. Unfortunately there are scant published data for sediments in the South China Sea Basin (McDermott et al., 1993; Solidum, 2002). Additionally, the sub-Philippines mantle has an Indian Ocean affinity and appears to host several different isotopic domains, as shown by the isotope composition of South China Sea floor basalts (see Figs. 5 and 6). Thus any quantifying calculations are necessarily rough as they rely on end-members that are difficult to characterize fully. Here we quantify sediment melt addition with Sr and Nd isotopes in a forward approach considering the caveats mentioned above. A sediment melt end-member is calculated with average South China Sea sediment data (McDermott et al., 1993) and bulk partition coefficients from Johnson and Plank (1999). The isotopic composition of the mantle end-member used is an average of published values for South China Seafloor basalts (Tu et al., 1992) which presumably represent the Bataan sub-arc mantle. Mantle Sr and Nd concentrations are from Sun and McDonough (1989). Simple mass balance calculations show that 1–5% of a small degree sediment melt ($F = 0.03$) added to the mantle wedge can explain the isotope data (see inset of Fig. 4). Alternatively, if bulk sediment is the more appropriate end-member, 1–3% is required (not shown in Fig. 4). Therefore, we consider the percentages derived from sediment melt mixing to be maxima.

In contrast to Bataan arc lavas, those from the Bicol arc have higher $^{143}Nd/^{144}Nd$, and lower $^{87}Sr/^{86}Sr$, yet still show steep linear arrays towards Pacific sediments in $^{207}Pb/^{204}Pb$ and $^{208}Pb/^{204}Pb$ vs. $^{206}Pb/^{204}Pb$ plots (Fig. 5). The linear trend in $^{207}Pb/^{204}Pb$ implicates sediment modification of the mantle wedge. Notably, the Pb isotope compositions of many Bicol lavas have less radiogenic values compared to those of the Philippine Sea basaltic crust (DSDP 291), which suggests a domain in the mantle wedge different from local Philippine basaltic crust and similar to mantle in the Palau Kyushu Ridge (Hickey-Vargas, 1991;

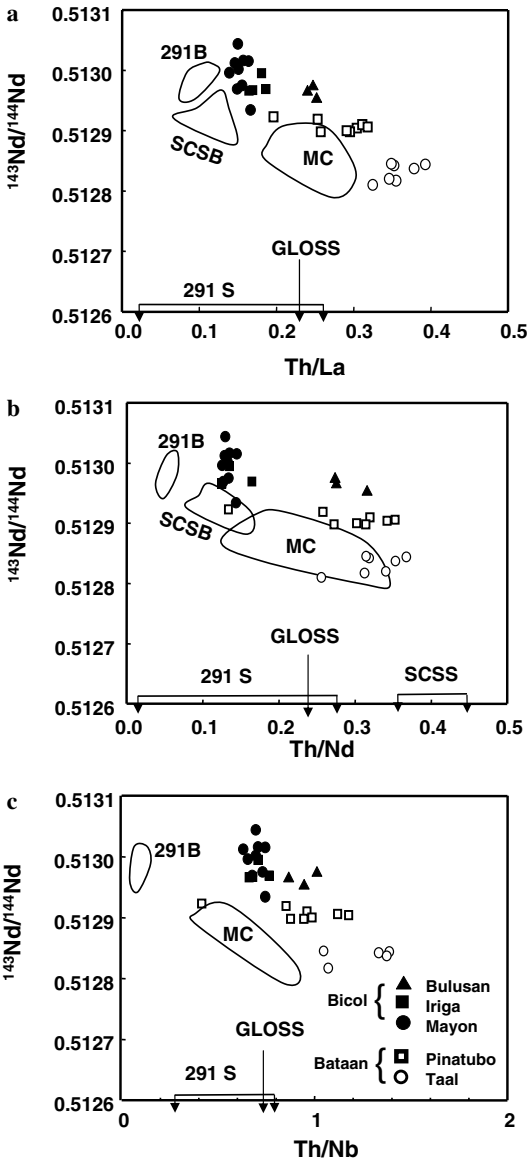

Fig. 7. (a) Th/La vs. $^{143}Nd/^{144}Nd$, (b) Th/Nd vs. $^{143}Nd/^{144}Nd$ and (c) Th/Nb vs. $^{143}Nd/^{144}Nd$ for Bicol and Bataan lavas. See the legend for an explanation of the symbols used. Shown for comparison (fields) are data from the Macolod Corridor (MC), South China Sea basalts (SCSB) and sediments (SCSS), DSDP drill hole 291 sediments (291S) and basalts (291B) and Global Subducted Sediment (GLOSS). In (a) Bicol lavas show a strong correlation towards 291S and towards GLOSS. Bataan lavas trend to values higher than 291S, although there is no Th/La data for SCSS. In (b) and (c) both Bicol and Bataan lavas are displaced to higher Th/Nb and Th/Nd than estimates for their mantle sources, which suggests sediments were transferred to the mantle as a melt phase (see text for discussion). Data sources are as follows: 291S (Solidum, 2002; Castillo and Newhall, 2004); 291B (Hickey-Vargas, 1998); SCSB (Tu et al., 1992); SCSS (Tu et al., 1992); MC (Knittel et al., 1997); GLOSS (Plank and Langmuir, 1998).

McDermott et al., 2004, 2005). Sediment addition is also indicated by high Th/La, similar to values for Philippine Sea sediments (Figs. 7 and 8a). In plots of Th/Nd and Th/Nb vs. $^{143}Nd/^{144}Nd$, Bicol arc data trend to higher Th/Nb and Th/Nd than data for Philippine Sea sediment, and adopting same reasoning as used for the Bataan data,

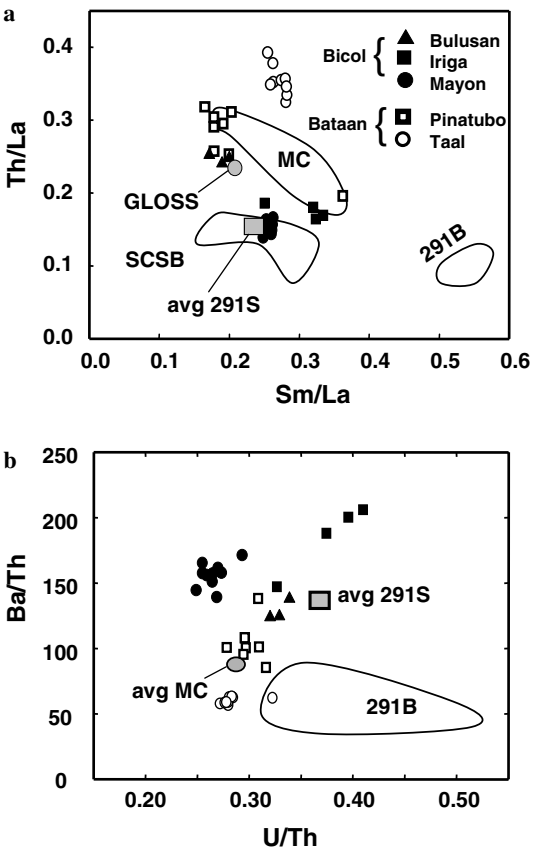

Fig. 8. Element ratio plots for Bicol and Bataan arc lavas. Symbols as in Fig. 7. Shown for comparison are data for the Macolod Corridor (MC), DSDP drill hole 291 basalts (291B) and sediments (291S), South China Sea basalts (SCSB), and Global Subducted Sediment (GLOSS). In (a) both Bicol and Bataan arcs show Th/La higher than estimates for their respective mantle sources, thus implicating sediment addition to the sub-arc mantle (see Plank, 2005). In (b) if the lavas from Mayon are ignored, there is a strong correlation between Ba/Th and U/Th, suggesting a fluid component is responsible for U enrichment for Iriga and Bulusan. Data from Taal and Pinatubo show less of a correlation (see text for discussion). Data sources are as follows: MC (Knittel et al., 1997); SCSB (Tu et al., 1992); 291S (Solidum, 2002; Castillo and Newhall, 2004); 291B (Hickey-Vargas, 1998); GLOSS (Plank and Langmuir, 1998).

it is likely that the sediment component was transferred to the mantle wedge as a melt phase (Castillo and Newhall, 2004; McDermott et al., 2004, 2005).

To quantify the sediment fraction added to the Bicol sub-arc mantle we use the same approach employed for the Bataan arc and calculate a hypothetical sediment melt end-member with isotope and trace element data from DSDP 291 sediments. The mantle end-member is slightly more problematic because published data for DSDP 291 basaltic crust has higher $^{87}Sr/^{86}Sr$ isotope ratios than measured in some Bicol lavas. Thus we choose a mantle end-member that is similar in composition to basalts from the Palau Kyushu Ridge (Hickey-Vargas, 1991; McDermott et al., 2004, 2005) and more closely resembles a simple depleted mantle. Mass balance calculations show that addition of 2–5% sediment melt can explain the isotope data.

Given the significant differences in sediment thicknesses between the two arcs, it is surprising that relative fraction of sediment required to explain the arc data is similar in both cases. One of the salient findings of this study, as shown above, is that sediment addition does not seem to be supply limited. Thus sediment transfer to the mantle wedge is likely controlled mechanically or by the thermal budget required to reach the sediment solidus, regardless of the supply at the trench. It follows that most subducted sediments are not sampled by the volcanic front and are either accreted, reside in the arc lithosphere, or are recycled into the convecting mantle. Though, it is more likely that sediments are transferred to the lithosphere or accreted, given the overall depleted composition of the mantle as sampled by MORBs.

5.1.2. Fluid addition

Lavas from the Bataan arc have low Ba/Th ratios (50–120), which are well-correlated with Sr and Nd isotopes. Taal volcano has the lowest Ba/Th ratios for this data set, typically ~50, and also the lowest Nd and highest Sr isotope ratios. High Ba/Th ratios typical of island arcs are thought to result from fluid-mediated enrichment from the subducting slab and are most clearly expressed at convergent margins that have extensively depleted mantle wedges facilitated by back arc spreading (see the Tonga-Kermadec and Marianas data in Fig. 6). However, low Ba/Th ratios of the Bataan rock suite are more akin to arcs where the sediment component dominates the trace element budget of the lavas, and which largely overprints any fluid-mediated enrichment. In spite of a strong sediment signature, Taal and Pinatubo rock suites consistently have (^{230}Th/^{238}U) activities less than unity (Fig. 9), which could be the result of fluid addition. Alternatively the relatively small ^{238}U activity excesses could be the result of decompression melting in the spinel stability field, as D_U/D_{Th} in clinopyroxene should be <1 with decreasing pressures (LaTourrette and Burnett, 1992; Beattie, 1993a; Wood et al., 1999). We explore this possibility more fully in Section 5.2; however, we believe that fluid addition is a more likely explanation for the ^{238}U activity excesses. Data from Taal show Ce/Pb and ^{207}Pb/^{204}Pb correlations that trend towards a low Ce/Pb, low ^{207}Pb/^{204}Pb end-member (see Fig. 8c in Castillo and Newhall, 2004), which likely represents fluid derived from basaltic ocean lithosphere (Miller et al., 1994; Brenan et al., 1995a). Also, a plot of ^{208}Pb*/^{206}Pb* vs. Th/U can discriminate between recent and long term U enrichment. Although the Taal and Pinatubo suites plot within the mantle array, data from the Macolod Corridor encompass those from Taal and Pinatubo, indicating recent U enrichment (Fig. 10). Thus there is evidence for fluid involvement in the Bataan arc that may be responsible for ^{238}U activity excesses.

Bicol lavas have Ba/Th ratios in the range of 120–200 which also correlate well with Sr and Nd isotope ratios (Fig. 6). The Bicol data form a broad positive array in plots of U/Th vs. Ba/Th that is exceptionally good if we exclude

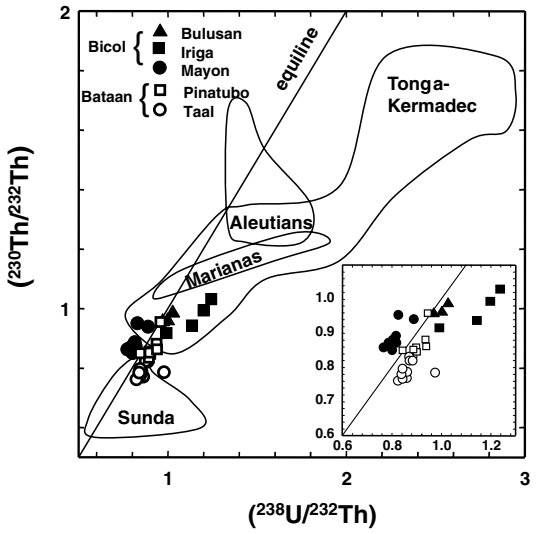

Fig. 9. U-series isotope equiline diagram for Bicol and Bataan lavas. See the legend for symbol explanation. Shown for comparison are data from selected arcs; inset shows greater detail. Iriga shows the greatest ^{238}U enrichment, and with its high Ba/Th ratios (Fig. 8) is consistent with fluid addition causing ^{238}U excess. Mayon has consistent ^{230}Th activity excesses and has lower (^{230}Th/^{232}Th) than the other Bicol lavas. Bataan lavas have lower (^{230}Th/^{232}Th) that those from Bicol. Data sources are as follows: Tonga-Kermadec (Turner et al., 1997); Aleutians (George et al., 2003); Marianas (Elliott et al., 1997); Sunda (Turner and Foden, 2001).

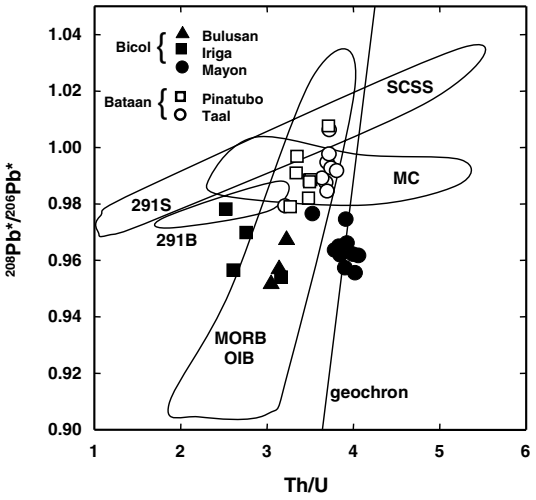

Fig. 10. ^{208}Pb*/^{206}Pb* vs. Th/U diagram which shows data for the Bicol and Bataan arcs. Closed and open circles represent data from the Bicol and Bataan arcs, respectively. Shown for comparison are compositional fields for Philippine Sea sediments (PSS), South China Sea sediments (SCSS), Macolod Corridor (MC), DSDP drill-hole 291 basalts (291B) and MORB and OIB. Recent U and Th enrichment should result in a horizontal array, compared to long term enrichment, which would show a vertical array. Bataan lavas are within the array of MORB and OIB; however, data from the MC encompass these and cross the MORB-OIB array (see text for discussion). Bicol lavas form an array that crosses the mantle array, suggesting that Th or U enrichment was recent. Data sources are as follows: PSS (Solidum, 2002; Castillo and Newhall, 2004); SCSS (McDermott et al., 1993); 291B (Hickey-Vargas, 1998); MORB-OIB (Bourdon et al., 2003) and references therein; MC (Knittel et al., 1997).

the Mayon data (Fig. 8b). Both of these observations suggest fluid addition, as Ba/Th of ~200 is high for a simple depleted mantle inferred to represent the Bicol sub-arc mantle. Furthermore, Ce/Pb and $^{207}Pb/^{204}Pb$ data point to a fluid derived from basaltic oceanic lithosphere as argued above for the Bataan data (see Fig. 8c in Castillo and Newhall, 2004) and a plot of $^{208}Pb^*/^{206}Pb^*$ vs. Th/U shows an extended range that plots perpendicular to the mantle array, indicating recent U enrichment (Fig. 10).

In summary, sediment addition in each arc is shown clearly by steep linear arrays that trend toward sediment values in $^{207}Pb/^{204}Pb$ vs. $^{206}Pb/^{204}Pb$ plots. Th/Nd and Th/Nb ratios that trend to higher values than the sediment end-members indicate that at least some of the sediment component was added as a partial melt. Finally, the Sr–Nd isotope composition of both Bicol and Bataan arc lavas can be explained by the addition of 1–5% sediment melt to the mantle wedge. Evidence for fluid addition is shown by Ce/Pb and $^{207}Pb/^{204}Pb$ data which suggest that the mantle mixed with a fluid derived from basaltic crust for both arcs. Additionally, the high Ba/Th ratios of Iriga and Bulusan positively correlate with U/Th, suggesting a role for fluid-mediated enrichment. We thus infer that fluid addition is largely responsible for the ^{238}U activity excesses observed in both arcs.

5.2. Peridotite melting and U-series isotopes

^{230}Th activity excesses measured in the Mayon rock suite are not observed in other lavas from the Bicol arc; neighboring Iriga and Bulusan have ^{238}U activity excesses. Mayon lavas also have Ba/Th ratios of ~150—among the highest measured (only Iriga has higher Ba/Th)—although these are modest when compared to the global arc data set (see Fig. 6). Given that high Ba/Th ratios and ^{238}U activity excesses are thought to reflect the addition of a fluid enriched in Ba and U to the source region, the processes which are responsible for Ba and U enrichment (e.g., fluid transfer) are likely different from those responsible for ^{230}Th activity excesses in Mayon lavas. The combined Bicol U-series data form a coherent array that crosses the equiline in Fig. 9. Relationships of this nature can be seen in other arc data (Elliott et al., 1997; Turner et al., 1997, 1998; Dosseto et al., 2003), and thus the processes that create the arrays in Fig. 9 likely occur beneath other subduction zones. There are at least three conditions that can create the observed patterns in Fig. 9: (1) the addition of a U-bearing fluid that contained some Th; (2) addition of a U-bearing fluid that contained no Th, followed by ageing; or (3) some combination of the effects of fluid addition and partial melting. The most straightforward interpretation, especially in very depleted arcs, has been the ageing of a Th-poor fluid because the solubility of Th is extremely low in aqueous fluids relative to U (Brenan et al., 1994, 1995b; Keppler, 1996). However, the effects of arc melting processes on U-series systematics have been relatively under-investigated, and thus we focus on mechanisms that could create these correlations other than simple fluid addition and ageing.

The relatively small ^{238}U excesses of Bulusan, Taal, and Pinatubo might be explained by low pressure decompression melting of spinel peridotite, as bulk D_U/D_{Th} is predicted to be <1 at decreasing pressures above the garnet stability field (LaTourrette and Burnett, 1992; Beattie, 1993a; Wood et al., 1999; McDade et al., 2003). We investigate this hypothesis with simple batch-melting of a spinel lherzolite source. The degree of ^{238}U activity excess produced (0.97–0.99) is much less than observed (0.8–0.95), even with bulk D_U/D_{Th} of 0.88 for 10% melting. Thus the U-series disequilibria observed is most likely inherited from a deeper part of the mantle that has been affected by fluids from the slab. One might also envision partial melting of mafic lower crust at even lower pressures (~0.8 GPa). However, Berlo et al. (2004) have shown U-series disequilibria produced from this process are also much lower than those observed in this study and globally, particularly for ($^{226}Ra/^{230}Th$) disequilibria. Basalts from Taal have ($^{226}Ra/^{230}Th$) = 1.6–1.4 (Asmerom et al., 2005), much higher than predicted by Berlo et al. (2004). Thus we infer that low pressure melting processes, either in the mantle or lower crust, are an unlikely explanation for the U series disequilibria measured in Bulusan, Taal, and Pinatubo lavas.

An ingrowth model that simulates partial melting of garnet peridotite, such as used to model ^{230}Th activity excess in MORB suites, is a more likely explanation. Because bulk D_U/D_{Th} is >1 in garnet-bearing peridotite (Beattie, 1993b), melting effects would counterbalance the effects of fluid addition to varying extents. Such reasoning may explain both the LILE enrichment and the ^{230}Th activity excesses of Mayon lavas. To investigate this scenario, we use a simple dynamic melting model (Williams and Gill, 1989) which simulates a one-dimensional upwelling mantle column. We assume that the amount of U addition is variable along the arc and that the pre-melted source is not in ($^{230}Th/^{238}U$) secular equilibrium. Other modeling parameters are given in the caption to Fig. 11. Mantle upwelling rates of between 2 and 6 cm yr^{-1} (melting rate = 1.41–4.24×10^{-4} kg m^{-3} yr^{-1}), shown by the lines in Fig. 11, can simulate both Bicol and Bataan arc data. Also, moderate ^{226}Ra activity excesses of ~1.5 observed in Mayon lavas (Turner et al., 2001) are consistent with an origin by melting and are not necessarily caused by fluid enrichment. Thus, one possible interpretation is that initial fluid addition caused ^{238}U enrichment, followed by dynamic decompression melting at different upwelling rates that increased the ($^{230}Th/^{232}Th$) of the aggregated melt. It is intriguing that the implied upwelling rates of 2–6 cm yr^{-1} correspond with estimated convergence rates (4.8–6.4 cm yr^{-1}). This would imply that mantle upwelling rates (and slab wedge decoupling) are identical to or slightly less than estimated convergence rates.

Another ingrowth model, perhaps more suitable for subduction zones, simulates packages of convecting mantle that are fluxed and melted at different levels in the arc

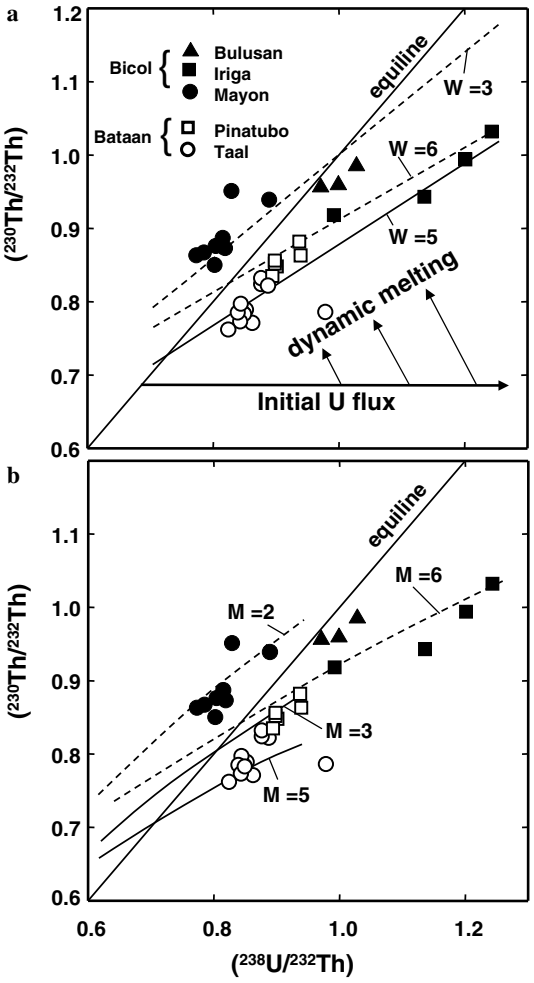

Fig. 11. Melt modeling of U-series isotopes using (a) the dynamic melting equations of Williams and Gill (1989) and (b) the continuous flux model of Thomas et al. (2002). Closed and open circles represent data from the Bicol and Bataan arcs, respectively. Solid and dashed lines represent model outputs using an initial (^{230}Th/^{232}Th) of 0.6 and 0.7, respectively. In (a) an initial U flux moves the source out of secular equilibrium (off the equiline). Subsequent dynamic melting at various upwelling rates (W in cm yr^{-1}) reproduces the data. In (b) fluids are continuously added to the mantle peridotite and melts are continuously extracted from all levels in the melting zone (see text for discussion). Variations in both the composition of the fluid flux and the melting rate are needed to reproduce the data trends. Melting rates (M) are shown in g m^{-3} y^{-1}. In both models ^{230}Th excesses require a lower U flux and lower melting rates. Model inputs (a) Mantle: Th = 0.19 ppm, U is varied to achieve secular disequilibrium; (b) Th = 0.19 ppm, U = 0.05 ppm, dU/df = 50–200 ppb. Bulk partition coefficients used in both models are 0.0034 and 0.00126 for U and Th, respectively, calculated assuming a mantle source of 8% garnet, 10% clinopyroxene, 30% orthopyroxene, and 52% olivine with partition coefficients from Salters and Longhi (1999). Critical porosity and degree of melting are 0.01 and 0.15, respectively for each model.

melting region. Following a melting episode, melt is removed from all the levels in the partially molten region, mixed, and then erupted to the surface instantaneously. U is added to each package of mantle via fluids, and therefore each package of mantle has variable degrees of U enrichment. Not all U is extracted in the melt, thus allowing for ^{230}Th ingrowth between melting stages in the mantle residue (Thomas et al., 2002; Bourdon et al., 2003). The major conceptual difference of this model is that the erupted magma is a mixture of melts from mantle sources that have experienced different melting histories and thus varying degrees of ^{230}Th ingrowth. This seems physically to be the more realistic model in that it simulates flux melting in a downward moving mantle. However, the effect on U-series disequilibria is similar to dynamic melting. We also assume melting of garnet peridotite and that the U-flux varies along the arc, from 50 to 200 ppb, which is a parameter that can be set directly in the model. The Bicol data can be reproduced with different melting rates, from 2–6 $\times$ 10^{-4} kg m^{-3} yr^{-1} at various effective degrees of melting (1–15%). Lavas from Mayon require lower melting rates ($\sim$2–3 $\times$ 10^{-4} kg m^{-3} yr^{-1}) and U fluxes ($\sim$50 ppb) to match the data while Iriga and Bulusan require larger U fluxes ($\sim$200 ppb) and faster melting rates ($\sim$6 $\times$ 10^{-4} kg m^{-3} yr^{-1}). Bataan arc data can be reproduced with a similar range in melting rates (3-5 $\times$ 10^{-4} kg m^{-3} yr^{-1}) but lower U fluxes (120 ppb). A major control on the slope of the model lines in Fig. 11b is the melting rate (M). At lower melting rates the slope will be steeper and vise versa, which is a direct consequence of longer timescales between melting pulses, thus allowing for more pronounced U-series ingrowth. The critical porosity has a similar effect on slope, although not as dramatic as the melting rate. Other modeling parameters are given in the caption to Fig. 11. We should stress that this model is only approximate, as some physical processes are not taken into account. For example, the fluid flux and fluid composition are assumed to be constant, whereas in reality both are likely to change as slab dehydration progresses. For further information about the mathematical treatment, the reader is referred to Thomas et al. (2002).

A key issue with the two ingrowth models proposed above is that they require the initial source (^{230}Th/^{232}Th) to be 0.6–0.7, as ingrowth processes increase the (^{230}Th/^{232}Th) activity ratio (McKenzie, 1985; Williams and Gill, 1989; Elliott et al., 1997). The mantle source could have had high Th/U ratios prior to any material addition from the subducting plate. However, lavas from the Bicol arc have low ^{207}Pb/^{204}Pb similar to the Palau Kyushu ridge and high ^{143}Nd/^{144}Nd–low ^{87}Sr/^{86}Sr which suggest long term depletion of incompatible elements. Lavas from Bataan have higher ^{87}Sr/^{86}Sr and lower ^{143}Nd/^{144}Nd, which is most likely the result of sediment addition as shown by ^{207}Pb/^{204}Pb values that trend towards South China Sea Sediments, rather than values consistent with an enriched mantle. If we assume that the unmodified sub-arc mantle is depleted, then the initial (^{230}Th/^{232}Th) should be between 0.8 and 1.35, which is a reasonable range for depleted mantle as sampled by MORBs. U/Th element data from local seafloor basalts (Hickey-Vargas, 1991) suggest that the (^{230}Th/^{232}Th) of the local mantle is $\sim$1.05. An instantaneous melting model, where U/Th fractionation is due solely to matrix-melt partitioning followed by decay, could lower the Th isotope composition.

However, ^{231}Pa activity excesses and ^{226}Ra activity excesses (Asmerom et al., 2000, 2005; Turner et al., 2001) are not consistent with this model. Thus the low (^{230}Th/^{232}Th) values required are most easily explained by mixing with sediments that have high Th/U, and thus low (^{230}Th/^{232}Th) if secular equilibrium is assumed.

The average (^{230}Th/^{232}Th) of DSDP 291 sediments, inferred from the Th/U ratio, is ~1.15 (Castillo and Newhall, 2004), which is higher than any of the Bicol Arc lavas. While at first it may seem impossible that such sediments could lower the isotope composition of the source, it is not certain whether there are compositional variations in the sediments along the arc length because of limited drill-hole coverage. Typical pelagic sediments have a (^{230}Th/^{232}Th) composition of ~0.6, and sediments from the South China Sea range from 0.45–1.34. Thus it is possible that the composition of DSDP 291 sediments is not wholly representative of subducted sediments along the Bicol arc, at least with respect to U and Th. Additionally, partial melting of sediment may result in a liquid with Th over U enrichment, depending on residual mineralogy. If sediment melting occurs over a timescale comparable to the half life of ^{230}Th, the outcome might be a component with lower (^{230}Th/^{232}Th). So we infer that the sediment component in the Bicol arc had high Th/U, thus lowering the (^{230}Th/^{232}Th) of the mantle source.

Two main inferences can be made from the above ingrowth models. First, the samples in the Bicol arc suite can be related by melting processes that operate on a timescale much longer than the half life of ^{230}Th, either by fluxing followed by dynamic decompression melting or by repeated mantle fluxing and mixing of melts from different levels in the mantle wedge. Thus, any age significance assigned to the inclined arrays on the U–Th equiline diagram must be interpreted with caution. Such inclined arrays have been interpreted as "dating" the time since fluids left the slab in highly depleted arcs (e.g. Turner et al., 1997, 2001; Bourdon et al., 1999, 2003). We infer that in less-depleted settings, melting processes can have a strong influence on U-series systematics. Second, we have shown that a dynamic "ingrowth" process can recreate the Bicol arc data, and the rates of these dynamic models correspond reasonably with estimated tectonic convergence rates. This provides at least some confidence that the dynamic ingrowth models may have validity and that partial melting is broadly proportional to plate convergence rate, which essentially dictates the rate of mantle matrix flow. In addition to the variations seen within the Bicol arc suite, a global negative correlation between the rate of plate convergence and average arc (^{230}Th/^{238}U) activity ratio agrees with this model (Fig. 12). Island arcs with slower convergence rates tend to have less extreme ^{238}U activity excess, consistent with a slow dynamic melting process that allows time for ^{230}Th ingrowth in the residue. Conversely, arcs with faster convergence rates do not allow enough time for ^{230}Th ingrowth in the mantle residue, and so tend to have greater ^{238}U activity excesses. We wish to stress that in these preliminary stages of assessing the problem devised models are still simplistic, as certainly the U and Th budgets of island arcs can be influenced by material addition from the subducting slab and by prior depletion of the mantle wedge. For instance the mantle wedge of the Tonga arc in Fig. 12 has been extensively depleted because of back arc spreading, and hence the large ^{238}U excess can largely be explained by fluid addition to an extremely depleted mantle. Also, the sediment-dominated arcs (grey circles in Fig. 12) could largely be explained by the dramatic effect of sediment addition that overwhelms any effect of a fluid component. However, even ignoring these extremes the correlation still exists, which allows us to infer that at least part of the correlation is controlled by the rate of mantle matrix flow, dictated by plate convergence rate.

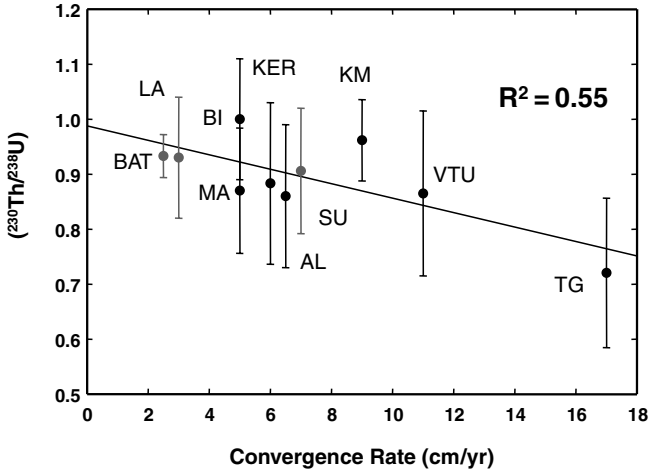

Fig. 12. Average (^{230}Th/^{238}U) vs. plate convergence rate (cm yr^{-1}) for global arcs and for lavas from this study. BAT = Bataan, LA = Lesser Antilles, BI = Bicol, MA = Marianas, KER = Kermadec, AL = Aleutians, SU = Sunda, KM = Kamchatka, VTU = Vanuatu, TG = Tonga. There is a broad negative correlation between the degree of ^{238}U excess and the rate of plate convergence, even if highly depleted and sediment dominated (grey symbols) arcs and not considered. To some extent the variation is likely due to U and/or Th contributions from the slab. However, some of the correlation may be controlled by the matrix flow rate, and hence the rate of convergence. Data sources are as follows: Bataan and Bicol, this study; Lesser Antilles (Turner et al., 1996); Marianas (Elliott et al., 1997); Tonga-Kermadec (Turner et al., 1997); Sunda (Turner et al., 2001); Kamchatka (Turner et al., 1998; Dosseto et al., 2003); Vanuatu (Turner et al., 1999).

5.3. Flux ingrowth vs. dynamic decompression melting

Davies and Stevenson (1992) have suggested that significant upwelling could occur in the mantle wedge if there is decoupling between the slab and mantle. In the case of the Bicol arc, upwelling rates would be less than or equal to estimates of plate convergence. Upwelling may be due to buoyancy contrasts resulting from a decrease in mantle viscosity caused by the presence of fluids (Davies and Stevenson, 1992), by diapiric upwelling of melt (Tatsumi, 1989; Davies and Stevenson, 1992; Kincaid and Sacks, 1997; Hall and Kincaid, 2001), or by increasing depletion of the

source. Yet as both Davies and Stevenson (1992) and Bourdon et al. (2003) point out, such scenarios are not likely to achieve steady state, which is assumed in many time-dependent melting models. Alternatively, the need for upwelling is not required for a continuously fluxed and melted mantle. Although the data presented here cannot distinguish between these two possibilities, some first order insights can be gleaned from the modeling exercises.

Results from both models imply melting rates of $\sim 10^{-4}$ kg m^{-3} yr^{-1}, consistent with estimates of crustal growth rates and petrologic models (Reymer and Schubert, 1984; Davies and Bickle, 1991). Also moderate ^{226}Ra activity excesses of Mayon lavas do not require rapid transport or melting rates to preserve large excesses induced by fluid addition at the slab mantle interface. Thus, choosing which model is the most appropriate or physically plausible is difficult. Bourdon et al. (2003) point out that to develop large Pa excesses, a continuous flux ingrowth model requires long melting timescales, on the order of several million years, to allow ^{231}Pa and ^{230}Th ingrowth in the mantle residue, which corresponds to a melting zone dimension of several hundred kilometers for a subduction rate of 10 cm yr^{-1}. This assumes that Pa and Th are immobile in fluids, which has support from many fluid mineral partitioning studies (Brenan et al., 1994, 1995b; Keppler, 1996). Yet, for subduction rates and angles estimated for the Bicol arc (5 cm yr^{-1} and 24°), a melting timescale of 4 Ma requires a melting zone dimension of ~82 km[1] (equal to ~200 km[1] of subducted slab), which is much more plausible and, interestingly, translates to estimated slab lengths beneath the Bicol arc of ~120–230 km (Cardwell et al., 1980; Besana et al., 1997). Such length-scales would produce large ^{231}Pa activity excesses of nearly 60% with the effective degree of melting equal to 0.15. Alternatively, melting timescales are greatly reduced if some Th and Pa are added to the wedge by fluids throughout the melting process, as suggested by both Reagan et al. (1994) and Thomas et al. (2002) for Central American lavas. The long-term average subduction rate is between ~4.8–6.4 cm yr^{-1} for the Bicol arc, which implies an appropriate melting region length-scale to allow for ^{231}Pa and ^{230}Th ingrowth via a continuous flux model.

Dynamic decompression melting has been considered inappropriate for modeling arc melting (e.g., Bourdon et al., 2003; Dosseto et al., 2003). This is because large ^{226}Ra excesses, thought to be related to fluid addition, are inconsistent with the premise that melt and matrix continuously equilibrate upon ascent (Turner et al., 2000, 2001; Bourdon et al., 2003). Thus the slow process of dynamic decompression melting would not preserve large ^{226}Ra activity excesses initiated at the slab–mantle interface. However, such restrictions seem to be more relaxed for Mayon lavas given the moderate (^{226}Ra/^{230}Th) activities of ~1.5 (Turner et al., 2001), which could have an origin through melting processes, and not necessarily through fluid-mediated enrichment. Consistent ^{230}Th and ^{231}Pa activity excesses imply that melting plays a significant role in controlling U-series systematics and thus, from a geochemical standpoint, dynamic decompression melting may be a viable melting mechanism for this arc.

[1] Determined by the relationship for a right triangle: $\sin\theta = y/r$, where y is segment opposite angle θ, and r is hypotenuse.

6. Conclusions

The Philippine arcs offer a unique opportunity to study arc melting and mass transfer processes, as the archipelago is bounded by subduction zones with contrasting sediment characteristics. From this study we derive the following conclusions:

(1) Addition of both sediment and fluid to each arc is implicated by high Th/La, ^{207}Pb/^{204}Pb vs. ^{206}Pb/^{204}Pb and Ce/Pb data. Th/Nb and Th/Nd ratios are higher than estimates of the mantle source, suggesting that the sediment component was likely added to the mantle as a melt phase and ~1–5% addition of sediment melt can explain the Sr–Nd isotope data. A significant finding of this study is that sediment addition to arc lavas is not controlled by sediment supply, but is rather thermally or mechanically limited. It follows that most sediment is not sampled by the volcanic front and is either accreted or resides in the arc lithosphere. It is unlikely that the majority of sediments are recycled into the upper convecting mantle, given the present day composition of MORBs.

(2) U–Th isotopes of both the Bicol and Bataan arcs can be related by a melting process that allows for ^{230}Th ingrowth, either dynamic melting of a source initially not in secular equilibrium or continuous mantle fluxing and melt extraction, provided that the source (^{230}Th/^{232}Th) was initially ~0.6–0.7. This can be explained easily by addition of 1–5% sediment melt to the source. Regardless of which model is more appropriate, the melting rate will control the extent of ^{230}Th ingrowth, which is ultimately controlled by the plate convergence rate. This is seen in a comparison of global arc data. It follows that inclined arrays on the U–Th equiline diagram likely reflect a component of ingrowth rather than the timing of U enrichment of the mantle wedge, and thus are unlikely to have chronological significance.

(3) Large upwelling rates or extremely low porosities are not required to explain the moderate (^{226}Ra/^{230}Th) activities in lavas from Mayon volcano. Moderate ^{230}Th activity excesses and large ^{231}Pa activity excesses measured in Mayon lavas suggest that melting processes play a significant role in controlling U-series isotope systematics in addition to the effects of fluid/sediment enrichment.

Acknowledgments

We are grateful to Ernesto Garcia Corpuz and other colleagues at the Philippine Institute of Volcanology and Seismology (PHIVOLCS), who assisted us with logistics,

provided invaluable information on local geology, and overall made the project possible. We appreciate the patient and thorough reviews of A. Stracke, P. Castillo, S. Galer, and one anonymous reviewer. We also thank Kirsten Menking and Janine Kennedy for proofreading the manuscript. The work was supported by National Science Foundation Collaborative Research Grant EAR-0208095 to Asmerom, EAR-0207830 to Mukasa, and EAR-0207429 to Morris.

Associate editor: Stephen J.G. Galer

References

Aguila, L.G., Newhall, C.G., Miller, D.M., Listanco, E.L., 1986. Reconnaissance geology of a large debris avalanche from Iriga volcano, Philippines. *Philip. J. Volc.* **3**, 54–72.

Argus, D.F., Gordon, R.G., 1991. No-net-rotation model of current plate velocities incorporating plate motion model NUVEL-1. *Geophys. Res. Lett.* **18**, 2039–2042.

Asmerom, Y., 1999. Th-U fractionation and mantle structure. *Earth Planet. Sci. Lett.* **166**, 163–175.

Asmerom, Y., Edwards, R.L., 1995. U-series isotope evidence for the origin of continental basalts. *Earth Planet. Sci. Lett.* **134**, 1–7.

Asmerom, Y., Mukasa, S., Cheng, H., Edwards, R.L., 2000. Pa–Th–U constraints on melting and material recycling in subduction zones: a case study of the Philippine arcs. *Goldschmt. Conf. Abstr.* **5** (2), A166.

Asmerom, Y., DuFrane, S.A., Mukasa, S.B., Cheng, H., Edwards, R.L., 2005. Time scale of magma differentiation in arcs from protactinium–radium isotopic data. *Geology* **33**, 633–636.

Beattie, P., 1993a. The generation of uranium series disequilibria by partial melting of spinel peridotite: constraints from partitioning studies. *Earth Planet. Sci. Lett.* **117**, 379–391.

Beattie, P., 1993b. Uranium–thorium disequilibria and partitioning on melting of garnet peridotite. *Nature* **363**, 63–65.

Berlo, K., Turner, S., Blundy, J., Hawkesworth, C., 2004. The extent of U-series disequilibria produced during partial melting of the lower crust with implications for the formation of the Mount St. Helens dacites. *Contrib. Mineral. Petrol.* **148**, 122–130.

Besana, G.M., Negishi, H., Ando, M., 1997. The three-dimensional attenuation structures beneath the Philippine archipelago based on seismic intensity data inversion. *Earth Planet. Sci. Lett.* **151**, 1–11.

Bourdon, B., Turner, S., Allegre, C., 1999. Melting dynamics beneath the Tonga-Kermadec island arc inferred from ^{231}Pa–^{235}U systematics. *Science* **286**, 2491–2493.

Bourdon, B., Turner, S., Dosseto, A., 2003. Dehydration and partial melting in subduction zones: constraints from U-series disequilibria. *J. Geophys. Res.* **108**, 2291–2310.

Brenan, J.M., Shaw, H.F., Ryerson, F.J., 1995a. Experimental evidence for the origin of lead enrichment in convergent-margin magmas. *Nature* **378**, 46–54.

Brenan, J.M., Shaw, D.L., Phinney, D.L., Ryerson, J.F., 1994. Mineral–aqueous fluid partitioning of Nb, Ta, Hf, Zr, U, and Th: implications for high field strength element depletions in island arc basalts. *Earth Planet. Sci. Lett.* **128**, 327–339.

Brenan, J.M., Shaw, D.L., Ryerson, J.F., Phinney, D.L., 1995b. Mineral–aqueous fluid partitioning of trace elements at 900 °C and 2.0 GPa: constraints on the trace element geochemistry of mantle and deep crustal fluids. *Geochim. Cosmochim. Acta* **59**, 3331–3350.

Cardwell, B.L., Isacks, B.L., Karig, D., 1980. The spatial distribution of earthquakes, focal mechanism solutions, and subducted lithosphere in the Philippine and northeastern Indonesian islands. In: Hayes, D.E. (Ed.), *The Tectonic and Geological Evolution of Southeast Asian Seas and Islands*, vol. 23. American Geophysical Union, Washington, DC, pp. 1–35.

Castillo, P.R., 1996. Origin and geodynamical implication of the Dupal isotopic anomaly in volcanic rocks from the Philippine island arcs. *Geology* **24**, 271–274.

Castillo, P.R., Newhall, C.G., 2004. Geochemical constraints on possible subduction components in lavas of Mayon and Taal volcanoes, southern Luzon, Philippines. *J. Petrol.* **45**, 1089–1108.

Cheng, H., Edwards, R.L., Hoff, J., Gallup, C.D., Richards, D.A., Asmerom, Y., 2000. The half-lives of uranium-234 and thorium-230. *Chem. Geol.* **169**, 17–33.

Class, C., Miller, D.M., Goldstein, S.L., Langmuir, C.H., 2000. Distinguishing melt and fluid subduction components in Umnak volcanics, Aleutian arc. *Geochem. Geophys., Geosys.* **1**, doi: 1999GC000010.

Davies, J.H., Bickle, M.J., 1991. A physical model for the volume and composition of melt produced by hydrous fluxing above subduction zones. *Philos. Trans. R. Soc. London, A* **335**, 355–364.

Davies, J.H., Stevenson, D.J., 1992. Physical model of source region of subduction zone volcanics. *J. Geophys. Res.* **97**, 2037–2070.

Delfin, F.G., Panem, C.C., Defant, M.J., 1993. Eruptive history and petrochemistry of the Bulusan volcanic complex: implications for the hydrothermal system and volcanic hazards of Mt. Bulusan, Philippines. *Geothermics* **22**, 417–434.

DeMets, C., Gordon, R.G., Argus, D.F., Stein, S., 1994. Effect of recent revisions to the geomagnetic reversal time scale on estimates of current plate motions. *Geophys. Res. Lett.* **21**, 2191–2194.

Dosseto, A., Bourdon, B., Joron, J.L., Dupre, B., 2003. U–Th–Pa–Ra study of the Kamchatka arc: new constraints on the genesis of arc lavas. *Geochim. Cosmochim. Acta* **67**, 2857–2877.

Edwards, R.L., Beck, J.W., Burr, G.S., Donahue, D.J., Chapell, J.M.A., Bloom, A.L., Druffel, E.R.M., Taylor, F.W., 1993. A large drop in atmospheric ^{14}C/^{12}C and reduced melting in the Younger Dryas documented with ^{230}Th ages of corals. *Science* **260**, 962–968.

Elliott, T., Plank, T., Zindler, A., White, W., Bourdon, B., 1997. Element transport from slab to volcanic front at the Mariana arc. *J. Geophys. Res.* **102**, 14991–15019.

George, R., Turner, S., Hawkesworth, C., Morris, J., Nye, C., Ryan, J., Zheng, S.H., 2003. Melting processes and fluid and sediment transport rates along the Alaska–Aleutian arc from an integrated U–Th–Ra–Be isotope study. *J. Geophys. Res.* **108**, doi: 2002JB002027.

Gill, J.B., Williams, R.W., 1990. Th isotope and U-series studies of subduction-related volcanic rocks. *Geochim. Cosmochim. Acta* **54**, 1427–1442.

Govindaraju, K., 1989. Compilation of working values and sample descriptions for 272 geostandards. *Geostd. Newslett.* **13** (special issue), 1–114.

Hall, P.S., Kincaid, C., 2001. Diapiric flow at subduction zones: a recipe for rapid transport. *Science* **292**, 2472–2475.

Hamburger, M.W., Cardwell, B.L., Isacks, B.L., 1983. Seismotectonics of the northern Philippine island arc. In: Hayes, D.E. (Ed.), *The Tectonic and Geologic Evolution of Southeast Asian Seas and Islands*, vol. 27. American Geophysical Union, Washington, DC, pp. 1–23.

Hart, S.R., 1984. A large-scale isotope anomaly in the Southern Hemisphere mantle. *Nature* **309**, 753–757.

Hawkesworth, C., Ellam, R., 1989. Chemical fluxes and wedge replenishment rates along recent destructive plate margins. *Geology* **17**, 46–49.

Hawkesworth, C., Turner, S., McDermott, F., Peate, D., Van Calsteren, P., 1997. U–Th isotopes in arc magmas: implications for element transfer from the subducted crust. *Science* **276**, 551–555.

Hayes, D.E., Lewis, S.D., 1984. A geophysical study of the Manila Trench, Luzon, Philippines 1. crustal structure, gravity and regional tectonic evolution. *J. Geophys. Res.* **89**, 9171–9195.

Hickey-Vargas, R., 1991. Isotope characteristics of submarine lavas from the Philippine Sea: implications for the origin of arc and basin magmas of the Philippine tectonic plate. *Earth Planet. Sci. Lett.* **107**, 290–304.

Hickey-Vargas, R., 1998. Origin of the Indian Ocean-type isotopic signature in basalts from the Philippine Sea plate spreading centers: an assessment of local versus large-scale processes. *J. Geophys. Res.* **103**, 20963–20979.

Holden, N.E., 1990. Total half lives for selected nuclides. *Pure Appl. Chem.* **62**, 941–958.

Johnson, M., Plank, T., 1999. Dehydration and melting experiments constrain the fate of subducted sediments. *Geochem., Geophys., Geosys.* **1**, doi: 1999GC000014.

Keppler, H., 1996. Constraints from partitioning experiments on the composition of subduction-zone fluids. *Nature* **380**, 237–240.

Kincaid, C., Sacks, I.S., 1997. Thermal and dynamical evolution of the upper mantle in subduction zones. *J. Geophys. Res.* **102**, 12295–12315.

Knittel, U., Hegner, E., Bau, M., Satir, M., 1997. Enrichment processes in the sub-arc mantle: a Sr–Nd–Pb isotopic and REE study of primitive arc basalts from the Philippines. *Can. Min.* **35**, 327–346.

LaTourrette, T.Z., Burnett, D.S., 1992. Experimental determination of U and Th partitioning between natural and synthetic basaltic liquid. *Earth Planet. Sci. Lett.* **110**, 227–244.

McDade, P., Blundy, J.D., Wood, B.J., 2003. Trace element partitioning on the Tinaquillo lherzolite solidus at 1.5 GPa. *Phys. Earth Planet. Inter.* **139**, 129–147.

McDermott, F., Defant, M.J., Hawkesworth, C.J., Maury, R.C., Joron, J.L., 1993. Isotope and trace element evidence for three component mixing in the genesis of the northern Luzon arc lavas (Philippines). *Contrib. Mineral. Petrol.* **113**, 9–23.

McDermott, F., Delfin, F.G., Defant, M.J., Turner, S., Maury, R.C., 2004. Source compositional variability beneath the Bicol arc, the Philippines. *Geochim. Cosmochim. Acta* **11S**, A598.

McDermott, F., Delfin, F.G., Defant, M.J., Turner, S., Maury, R.C., 2005. The petrogenesis of volcanics from Mt. Bulusan and Mt. Mayon in the Bicol arc, the Philippines. *Contrib. Mineral. Petrol.* **150**, 652–670.

McKenzie, D., 1985. ^{230}Th–^{238}U disequilibria and the melting processes beneath ridge axes. *Earth Planet. Sci. Lett.* **72**, 149–157.

Miklius, A., Flower, M.F.J., Huijsmans, J.P.P., Mukasa, S., Castillo, P.R., 1991. Geochemistry of lavas from Taal volcano, southwestern Luzon, Philippines: evidence for multiple magma supply systems and mantle source heterogeneity. *J. Petrol.* **32**, 593–627.

Miller, D.M., Goldstein, S.J., Langmuir, C.H., 1994. Cerium/lead and lead isotope ratios in arc magmas and the enrichment of lead in the continents. *Nature* **368**, 514–520.

Morris, J., Hart, S.R., 1983. Isotopic and incompatible element constraints on the genesis of island arc volcanics from Cold Bay and Amak island, Aleutians, and implications for mantle structure. *Geochim. Cosmochim. Acta* **47**, 2015–2030.

Morris, J., Tera, F., 1989. ^{10}Be/^{9}Be in mineral separates and whole rocks from volcanic arcs: implications for sediment subduction. *Geochim. Cosmochim. Acta* **53**, 3197–3206.

Mukasa, S.B., McCabe, R., Gill, J.B., 1987. Pb-isotopic composition of volcanic rocks in the west and east Philippine island arcs: presence of the Dupal isotopic anomaly. *Earth Planet. Sci. Lett.* **84**, 153–164.

Mukasa, S.B., Flower, M.F.J., Miklius, A., 1994. The Nd, Sr, and Pb isotopic character of lavas from Taal, Laguna de Bay, and Arayat volcanoes, S.W. Luzon, Philippines: implications for arc magma petrogenesis. *Tectonophys.* **235**, 205–221.

Newhall, C.G., Daag, A.S., Delfin, F.G., Hoblitt, R.P., McGeehin, J., Pallister, J.S., Regalado, T.M., Rubin, M., Tubianosa, B.S., Tamayo, R.A., Umbal, J.V., 1996. Eruptive history of Mount Pinatubo. In: Newhall, C.G., Punongbayan, R. (Eds.), *Fire and Mud: Eruptions and Lahars of Mount Pinatubo Philippines*. University of Washington Press, Seattle, pp. 165–196.

Pearce, J.A., Parkinson, I.J., 1993. Trace element models for mantle melting: application to volcanic arc petrogenesis. In: Prichard, H.M., Alabaster, T., Harris, N.B.W., Neary, C.R. (Eds.), *Magmatic Processes and Plate Tectonics*. Geological Society, London, pp. 373–403.

Pickett, D.A., Murrell, M.T., 1997. Observations of ^{231}Pa/^{235}U disequilibria in volcanic rocks. *Earth Planet. Sci. Lett.* **148**, 259–271.

Plank, T., 2005. Constraints from thorium/lanthanum on sediment recycling at subduction zones and the evolution of the continents. *J. Petrol.* **46**, 921–944.

Plank, T., Langmuir, C.H., 1988. An evaluation of the global variations in the major element chemistry of arc basalts. *Earth Planet. Sci. Lett.* **90**, 349–370.

Plank, T., Langmuir, C.H., 1998. The chemical composition of subducting sediment and its consequences for the crust and mantle. *Chem. Geol.* **145**, 325–394.

Ramos-Villarta, S.C., Corpuz, E.G., Newhall, C.G., 1985. Eruptive history of Mayon Volcano, Philippines. *Philip. J. Volc.* **2**, 1–35.

Reagan, M.K., Gill, J.B., 1989. Coexisting calcalkaline and high niobium basalts from Turrialba volcano, Costa Rica: implications for residual titanates in arc magma sources. *J. Geophys. Res.* **94**, 4619–4633.

Reagan, M.K., Morris, J., Herrstrom, E.A., Murrell, M.T., 1994. Uranium series and beryllium isotope evidence for an extended history of subduction modification of the mantle below Nicaragua. *Geochim. Cosmochim. Acta.* **58**, 4199–4212.

Reymer, A., Schubert, G., 1984. Phanerozoic addition rates to the continental crust and crustal growth. *Tectonics* **3**, 63–77.

Robert, J., Miranda, C.F., Muxart, R., 1969. Mesure de la periode du protactinium-231 par microcalorimetrie. *Radiochim. Acta* **11**, 104–108.

Salters, V.J.M., Longhi, J.E., 1999. Trace element partitioning during the initial stages of melting beneath mid-ocean ridges. *Earth Planet. Sci. Lett.* **166**, 15–30.

Solidum, R.U., 2002. Geochemistry of volcanic arc lavas in central and southern Philippines: contributions from the subducted slab. Dissertation, University of California, San Diego.

Stolz, A.J., Varne, G.R., Davies, J.H., Wheller, G.E., Foden, J., 1990. Magma source components in an arc-continent collision zone: the Flores-Lembata sector, Sunda arc, Indonesia. *Contrib. Mineral. Petrol.* **105**, 585–601.

Sun, M., McDonough, W.F., 1989. Chemical and isotopic systematics of oceanic basalts: implications for mantle composition and processes. In: Saunders, A.D., Norry, M.J. (Eds.), *Magmatism in the Ocean Basins*, vol. 42. Geological Society of London, London, pp. 313–345.

Tatsumi, Y., 1989. Migration of fluid phases and genesis of basalt magmas in subduction zones. *J. Geophys. Res.* **94**, 4697–4707.

Tatsumi, Y., Hamilton, D.L., Nesbitt, R.W., 1986. Chemical characteristics of fluid phase released from a subducted lithosphere and origin of arc magmas: evidence from high pressure experiments and natural rocks. *J. Volcan. Geother. Res.* **29**, 293–309.

Tera, F., Brown, L., Morris, J., Sacks, I.S., Klein, J., Middleton, R., 1986. Sediment incorporation in island arc magmas: inferences from ^{10}Be. *Geochim. Cosmochim. Acta* **50**, 636–660.

Thomas, R.B., Hirschmann, M.M., Cheng, H., Reagan, M.K., Edwards, R.L., 2002. (^{231}Pa/^{235}U)–(^{230}Th/^{238}U) of young mafic volcanic rocks from Nicaragua and Costa Rica and the influence of flux melting on U-series systematics of arc lavas. *Geochim. Cosmochim. Acta* **66**, 4287–4309.

Tu, K., Flower, M.F.J., Carlson, R.W., Xie, G., Chen, C.Y., Zhang, M., 1992. Magmatism in the South China Basin 1. Isotopic and trace-element evidence for an endogenous Dupal mantle component. *Chem. Geol.* **97**, 47–63.

Turner, S., Foden, J., 2001. U, Th, and Ra disequilibria, Sr, Nd, and Pb isotope and trace element variations in Sunda arc lavas: predominance of a subducted sediment component. *Contrib. Mineral. Petrol.* **142**, 43–57.

Turner, S., Evans, P., Hawkesworth, C.J., 2001. Ultrafast source-to-surface movement of melt at island arcs from ^{226}Ra–^{230}Th systematics. *Science* **292**, 1363–1366.

Turner, S., McDermott, F., Hawkesworth, C., Kepezhinskas, P., 1998. A U-series study of lavas from Kamchatka and the Aleutians: constraints on source composition and melting processes. *Contrib. Mineral. Petrol.* **133**, 217–234.

Turner, S., Bourdon, B., Hawkesworth, C., Evans, P., 2000. ^{226}Ra–^{230}Th evidence for multiple dehydration events, rapid melt ascent and the time scales of differentiation beneath the Tonga-Kermadec island arc. *Earth Planet. Sci. Lett.* **179**, 581–593.

Turner, S., Peate, D., Hawkesworth, C., Eggins, S.M., Crawford, A.J., 1999. Two mantle domains and the time scales of fluid transfer beneath the Vanuatu arc. *Geology* **27**, 963–966.

Turner, S., Hawkesworth, C., Van Clasteren, P., Heath, E., Macdonald, R., Black, S., 1996. U-series isotopes and destructive plate margin magma genesis in the Lesser Antilles. *Earth Planet. Sci. Lett.* **142**, 191–207.

Turner, S., Hawkesworth, C., Rogers, N., Bartlet, J., Worthington, T., Hergt, J., Pearce, J., Smith, I., 1997. ^{238}U–^{230}Th disequilibria, magma petrogenesis, and flux rates beneath the depleted Tonga-Kermadec island arc. *Geochim. Cosmochim. Acta* **61**, 4855–4884.

Williams, R.W., Gill, J.B., 1989. Effects of partial melting on the uranium decay series. *Geochim. Cosmochim. Acta* **53**, 1607–1619.

Wood, B., Blundy, J., Jonathan, D., Robinson, J., 1999. The role of clinopyroxene in generating U-series disequilibria during mantle melting. *Geochim. Cosmochim. Acta* **63**, 1613–1620.